

Does Weak-to-strong Generalization Happen under Spurious Correlations?

Chenruo Liu*

Yijun Dong*

Qi Lei

New York University

{c17758, yd1319, q1518}@nyu.edu

Abstract

We initiate a unified theoretical and algorithmic study of a key problem in weak-to-strong (W2S) generalization: when fine-tuning a strong pre-trained student with pseudolabels from a weaker teacher on a downstream task with spurious correlations, does W2S happen, and how to improve it upon failures? We consider two sources of spurious correlations caused by group imbalance: (i) a weak teacher fine-tuned on group-imbalanced labeled data with a minority group of fraction η_ℓ , and (ii) a group-imbalanced unlabeled set pseudolabeled by the teacher with a minority group of fraction η_u . Theoretically, a precise characterization of W2S gain at the proportional asymptotic limit shows that W2S always happens with sufficient pseudolabels when $\eta_u = \eta_\ell$ but may fail when $\eta_u \neq \eta_\ell$, where W2S gain diminishes as $(\eta_u - \eta_\ell)^2$ increases. Our theory is corroborated by extensive experiments on various spurious correlation benchmarks and teacher-student pairs. To boost W2S performance upon failures, we further propose a simple, effective algorithmic remedy that retrains the strong student on its high-confidence data subset after W2S fine-tuning. Our algorithm is group-label-free and achieves consistent, substantial improvements over vanilla W2S fine-tuning.

1 Introduction

Traditional learning paradigms like supervised learning and knowledge distillation [Hinton et al., 2015] learn from training data generated by strong teachers, *e.g.*, human experts. In contrast, contemporary foundation models encode encyclopedic knowledge through astronomical-scale pre-training, thereby achieving comparable or even superior performance to human experts in various domains via light post-training adaptation like fine-tuning [Brown et al., 2020, Achiam et al., 2023]. This motivates the question on *superalignment* [Leike and Sutskever, 2023]: can models with superhuman intelligence learn from weaker human supervision? *Weak-to-strong (W2S) generalization* [Burns et al., 2024] provides an encouraging answer for this question: a strong pre-trained student fine-tuned with pseudolabels generated by a weaker teacher can often outperform its teacher.

Since the first introduction of W2S by Burns et al. [2024], its mechanism has been extensively studied empirically [Guo et al., 2024, Liu and Alahi, 2024, Guo and Yang, 2024, Yang et al., 2024, 2025, Goel et al., 2025], and theoretically [Lang et al., 2024, Charikar et al., 2024, Wu and Sahai, 2025, Ildiz et al., 2025, Mulgund and Pabbaraju, 2025, Dong et al., 2025, Medvedev et al., 2025].

*Equal contribution.

While existing works on W2S generally assume access to clean downstream data, in practice, both the weak teacher and the unlabeled data for weak supervision often carry systematic biases, such as spurious correlations tied to demographic or acquisition factors [Arjovsky et al., 2019, Sagawa et al., 2020].

This challenge is especially relevant in the very settings that motivate W2S: a student broadly pre-trained on general data is fine-tuned for a specialized task where labeled samples are scarce and imperfect. In medicine, labels may be biased toward certain patient groups [Gupta et al., 2016] or imaging devices [Zech et al., 2018]; in law, datasets may overrepresent particular jurisdictions or case types [Chalkidis et al., 2022]; in autonomous driving, sensor data may be skewed toward specific weather or traffic conditions [Liu et al., 2024]. For these specialized downstream tasks, one usually cannot interfere with the data acquisition process, nor obtain additional balanced data. It is therefore crucial to understand *whether W2S can remain effective under spurious correlations* caused by group imbalance—*when it succeeds, when it fails, and how its procedure can be improved*.

Our contributions. We initiate a systematic study of W2S under spurious correlations, providing (i) a theoretical analysis that answers the “when” question comprehensively by characterizing the impact of spurious correlations on W2S precisely in the proportional asymptotic limit, as well as (ii) a simple, effective remedy for the failure of W2S under spurious correlations inspired by our theory, toward answering the “how” question. Concretely, our contributions are as follows.

- **A theory of W2S under spurious correlations.** In Section 2, we conduct a systematic analysis in the ridgeless regression setting with zero approximation error, where W2S happens due to different estimation errors (*i.e.*, efficiency in utilizing data). At the proportional asymptotic limit, we provide *precise characterizations for the generalization errors of both teacher and student*. Consider using a weak teacher fine-tuned on labeled samples with a minority fraction η_ℓ to pseudolabel N unlabeled samples with a minority fraction η_u for W2S fine-tuning. We show that (i) *W2S always happens with sufficiently large N when $\eta_\ell = \eta_u$ and improves when the teacher and student have distinct representations*; whereas (ii) *when $\eta_\ell \neq \eta_u$, W2S can fail even with $N \rightarrow \infty$, and W2S gain tends to diminish as $(\eta_u - \eta_\ell)^2$ increases*. Our theory is validated with extensive experiments on synthetic regression problems and real classification tasks (Section 3).
- **An algorithmic enhancement for W2S when $\eta_\ell \neq \eta_u$.** In Section 4, we propose a simple, effective algorithm that retrains the strong student on its high-confidence data subset after W2S fine-tuning via the generalized cross-entropy loss [Zhang and Sabuncu, 2018]. Our method requires no group annotations and improves W2S when the gap between η_u and η_ℓ is large. We conduct extensive experiments on assorted spurious correlation benchmarks (e.g., Waterbirds [Sagawa et al., 2020], BFFHQ [Lee et al., 2021], and ImageNet-9 [Xiao et al., 2020]), across 10 different teacher–student model pairs. The results show that our algorithm achieves consistent and substantial gains over vanilla W2S.

1.1 Related Works

W2S generalization. Empirically, many methods have been developed to validate/enhance W2S across various vision and natural language modeling tasks, including adjustable loss functions [Guo et al., 2024], multi-teacher algorithms [Liu and Alahi, 2024], data refinement strategies [Guo and Yang, 2024, Yang et al., 2024], and the use of weak models for data filtering

[Li et al., 2024]. Theoretical work on W2S is also rapidly expanding, offering various mechanistic explanations from first principles, including the perspectives of neighborhood expansion [Lang et al., 2024], data overlap density [Shin et al., 2025], transfer learning [Somerstep et al., 2024], teacher-student disagreement [Charikar et al., 2024, Mulgund and Pabbaraju, 2025, Yao et al., 2025, Xu et al., 2025], benign overfitting [Wu and Sahai, 2025, Xue et al., 2025], knowledge distillation [Ildiz et al., 2025], low intrinsic dimension of fine-tuning [Aghajanyan et al., 2021, Dong et al., 2025], regularization [Medvedev et al., 2025, Moniri and Hassani, 2025], and feature learning with different inductive biases [Oh et al., 2025].

Group robustness to spurious correlation. Extensive efforts have been devoted to mitigating spurious correlation for robust and safe generalization to unseen test domains [Arjovsky et al., 2019, Sagawa et al., 2020, Krueger et al., 2021, Deng et al., 2023, Phan et al., 2024, Wen et al., 2025, Liu et al., 2025b]. Among these studies, a subset of work specifically targets spurious correlation arising from group imbalance. When group labels are available, canonical approaches include reweighting minority groups [Sagawa et al., 2020], downsampling majority groups [Deng et al., 2023], distributionally robust optimization [Sagawa et al., 2020, Zhang et al., 2020], and progressive data expansion [Deng et al., 2023]. Since obtaining group annotations in training data can be costly or even infeasible, alternative strategies aim to identify biased samples without explicit group supervision [Nam et al., 2020, Liu et al., 2021, Zhang et al., 2022, Yenamandra et al., 2023, Han and Zou, 2024], or leverage auxiliary signals such as knowledge of spurious attributes [Puli et al., 2021], class annotations [LaBonte et al., 2024], and superclass-level information [Liu et al., 2025a]. Unlike group robustness methods in (semi-)supervised learning, our setting addresses a different source of bias: pseudo-labels generated by a weak teacher. These pseudo-labels can inherit spurious correlations from two directions — (i) the labeled data on which the teacher itself was trained, and (ii) the unlabeled samples on which the teacher is applied. Our goal is to understand and improve how these two sources jointly affect W2S, making our analysis orthogonal to, and more intricate than, standard robustness approaches.

Group robustness in knowledge distillation. Knowledge distillation (KD) [Hinton et al., 2015] is closely related to W2S but with the roles reversed: KD transfers knowledge from a larger teacher model to a smaller student model. A series of works has analyzed when and why a distilled student generalizes [Phuong and Lampert, 2019, Stanton et al., 2021, Ojha et al., 2023, Nagarajan et al., 2023, Dong et al., 2024, Ildiz et al., 2025]. Analytically, W2S departs from traditional KD because “weak” vs. “strong” is defined relative to pretraining, so W2S is naturally studied as fine-tuning on pseudolabeled data.

When transferring knowledge from a strong teacher to a weaker student, knowledge distillation [Hinton et al., 2015] has been shown to harm the minority group performance [Lukasik et al., 2021, Vilouras et al., 2023, Wang et al., 2023, Lee and Lee, 2023, Kenfack et al., 2024]. To address this issue, different methods have been proposed, including adaptive mixing weights and per-class margins [Lukasik et al., 2021], distributionally robust optimization [Wang et al., 2023, Vilouras et al., 2023], last-layer transplantation [Lee and Lee, 2023], and gradient-based reweighting [Kenfack et al., 2024]. Our work differs from these approaches in three key aspects: (a) W2S generalization, where a weak teacher supervises a stronger student, is fundamentally distinct from classical knowledge distillation, (b) we explicitly consider the impact of mismatched minority group proportions between teacher and student, and (c) our method for improving W2S performance does not require any auxiliary information such as

group annotations.

2 A Theory of W2S under Spurious Correlation

Notations. For any $p, q \in \mathbb{N}$, $p \geq q$, let $\text{Stiefel}(p, q) = \{\mathbf{Q} \in \mathbb{R}^{p \times q} \mid \mathbf{Q}^\top \mathbf{Q} = \mathbf{I}_q\}$ be the Stiefel manifold. $\mathbf{A} \otimes \mathbf{B} \in \mathbb{R}^{mp \times nq}$ denotes the Kronecker product of $\mathbf{A} \in \mathbb{R}^{m \times n}$ and $\mathbf{B} \in \mathbb{R}^{p \times q}$; when $n = q$, let $[\mathbf{A}; \mathbf{B}] \in \mathbb{R}^{(m+p) \times n}$ be the vertical stack; when $m = p$, let $[\mathbf{A}, \mathbf{B}] \in \mathbb{R}^{m \times (n+q)}$ be the horizontal stack. For any $\mathbf{w} \in \mathbb{R}^d$ and $i \in [d]$ or $\mathcal{I} \subseteq [d]$, let w_i and $[\mathbf{w}]_{\mathcal{I}}$ denote the i -th entry and the subvector of \mathbf{w} indexed by \mathcal{I} . For any $\mathbf{A} \in \mathbb{R}^{m \times n}$ and $i \in [m], j \in [n]$, let $A_{i,j}$ denote the (i, j) -th entry; $[\mathbf{A}]_{i,:} \in \mathbb{R}^n$ denotes the i -th row; $[\mathbf{A}]_{:,j} \in \mathbb{R}^m$ denotes the j -th column; and index subsets $\mathcal{I} \subseteq [m], \mathcal{J} \subseteq [n]$ pick the corresponding submatrices.

2.1 Problem Setup: Regression under Spurious Correlation

Downstream task. Consider a downstream regression task characterized by a distribution $\mathcal{D}(\eta) : \mathcal{X} \times \mathcal{Y} \times \mathcal{G} \rightarrow [0, 1]$ where \mathcal{X} is the input space, $\mathcal{Y} = \mathbb{R}$ is the label space, and $\mathcal{G} = \{0, 1\}$ contains group labels (*i.e.*, 1 for minority and 0 for majority). The fraction of the minority group in the population is controlled by $\eta \in [0, \frac{1}{2}]$ such that $\Pr[g = 1] = 1 - \Pr[g = 0] = \eta$.

Assumption 1 (Regression under spurious correlations). *Let \mathcal{D}_x be the marginal distribution of $\mathbf{x} \in \mathcal{X}$; $\mathcal{D}_{x|g}$ be the conditional distribution of \mathbf{x} given g ; and $\mathcal{D}_{y|x}$ be the conditional distribution of y given \mathbf{x} satisfying $y = f_*(\mathbf{x}) + \epsilon$ for unknown $f_* : \mathcal{X} \rightarrow \mathbb{R}$ and i.i.d. label noise $\epsilon \sim \mathcal{N}(0, \sigma_y^2)$ independent of \mathbf{x} . Consider two feature maps: (i) the core feature $\mathbf{z} : \mathcal{X} \rightarrow \mathbb{R}^{d_z}$ determines the label y through $\mathbf{z}(\mathbf{x}) \sim \mathcal{N}(\mathbf{0}_{d_z}, \mathbf{I}_{d_z})$ and $f_*(\mathbf{x}) = \mathbf{z}(\mathbf{x})^\top \beta_*$ for fixed $\beta_* \in \mathbb{R}^{d_z}$; while (ii) the group feature $\xi : \mathcal{X} \rightarrow \mathbb{R}^p$ ($2 < p < \infty$) determines the group label g through $\xi(\mathbf{x}) \sim \mathcal{N}(g\mu_\xi, \sigma_\xi^2 \mathbf{I}_p)$ for fixed $\mu_\xi \in \mathbb{R}^p$ with dimension-independent $\|\mu_\xi\|_2, \sigma_\xi^2 \asymp 1$.*

Here, $\mathbf{z}(\mathbf{x})$ encodes the core information for predicting y that is invariant across groups, typically rich in semantics and therefore hard to learn (high-dimensional); while $\xi(\mathbf{x})$ is a latent feature controlling which group \mathbf{x} belongs to, typically simpler to represent and therefore low-dimensional.

Weak and strong models. We consider two pre-trained models that provide reasonably high-quality features for the downstream task: a weak teacher model $f_T : \mathcal{X} \rightarrow \mathbb{R}$ and a strong student model $f_S : \mathcal{X} \rightarrow \mathbb{R}$. Adapting the setting in Dong et al. [2025], we model fine-tuning in the kernel regime [Jacot et al., 2018, Malladi et al., 2023] with low intrinsic dimensions [Aghajanyan et al., 2021]. In particular, we consider learning overparametrized linear layers $\theta_T \in \mathbb{R}^{D_T}$ and $\theta_S \in \mathbb{R}^{D_S}$ over high-dimensional pre-trained representations $\varphi_T : \mathcal{X} \rightarrow \mathbb{R}^{D_T}$ and $\varphi_S : \mathcal{X} \rightarrow \mathbb{R}^{D_S}$, respectively. The pivotal assumption in this setting is the difference between φ_T, φ_S that separates the weak and strong models on the downstream task with spurious correlations:

Assumption 2 (Weak vs. strong models). (i) *The weak teacher representation φ_T heavily entangles the core and group features: there exists $\mathbf{U}_T \in \text{Stiefel}(D_T, d_T)$ ($d_T \ll D_T$) such that $\varphi_T(\mathbf{x}) = \mathbf{U}_T \phi_T(\mathbf{x})$ and $\phi_T(\mathbf{x}) = \mathbf{z}(\mathbf{x}) \otimes \mathbf{w}(\mathbf{x})$, where $\mathbf{w}(\mathbf{x}) = [1; \mathbf{T}^\top \xi(\mathbf{x})] \in \mathbb{R}^{p_T}$ ($2 \leq p_T \leq p$) for a fixed $\mathbf{T} \in \text{Stiefel}(p, p_T - 1)$ that projects $\xi(\mathbf{x})$ to a lower dimension (*i.e.*, $\phi_T(\mathbf{x}) = [\mathbf{z}(\mathbf{x}); \mathbf{z}(\mathbf{x}) \otimes (\mathbf{T}^\top \xi(\mathbf{x}))] \in \mathbb{R}^{d_T}$). We note that $d_T = p_T d_z$. Let $\mu_T = \mathbf{T}^\top \mu_\xi \in \mathbb{R}^{p_T-1}$.*

(ii) *A strong student representation φ_S partially disentangles the core and group features: there exists $\mathbf{U}_S \in \text{Stiefel}(D_S, d_S)$ ($d_S \ll D_S$) such that $\varphi_S(\mathbf{x}) = \mathbf{U}_S \phi_S(\mathbf{x})$ and $\phi_S(\mathbf{x}) = \mathbf{z}(\mathbf{x}) \otimes$*

$\psi(\mathbf{x})$, where $\psi(\mathbf{x}) = [1; \mathbf{S}^\top \xi(\mathbf{x})] \in \mathbb{R}^{p_S}$ ($2 \leq p_S \leq p_T$) for a fixed $\mathbf{S} \in \text{Stiefel}(p, p_S - 1)$ that projects $\xi(\mathbf{x})$ to a much lower dimension, $p_S \ll p$ (i.e., $\phi_S(\mathbf{x}) = [\mathbf{z}(\mathbf{x}); \mathbf{z}(\mathbf{x}) \otimes (\mathbf{S}^\top \xi(\mathbf{x}))] \in \mathbb{R}^{d_S}$). We note that $d_S = p_S d_z$. Let $\mu_S = \mathbf{S}^\top \mu_\xi \in \mathbb{R}^{p_S-1}$.¹

Assumption 2 formalizes the intuitions that compared to φ_T , the stronger φ_S (i) represents the information required for the downstream task more efficiently ($d_S \leq d_T$) and (ii) partially disentangles the core and group features, bringing robustness to spurious correlations. Notice that with $\mathbf{z}(\mathbf{x})$ prepending in both $\varphi_T(\mathbf{x})$ and $\varphi_S(\mathbf{x})$, the teacher and student both have zero approximation error (i.e., both pre-trained models are expressive enough for the downstream task), and W2S happens due to different estimation errors (i.e., the student is more sample efficient than its teacher).

Example 1. Taking the Waterbirds dataset [Sagawa et al., 2020] as an example: with $\mathbf{z}(\mathbf{x})$ encoding the foreground of birds, $\xi(\mathbf{x})$ represents whether the background is typical or not, while $\mathbf{z}(\mathbf{x}) \otimes \mathbf{w}(\mathbf{x})$ and $\mathbf{z}(\mathbf{x}) \otimes \psi(\mathbf{x})$ correspond to the representations of background from the weak and strong models.

While the Platonic representation hypothesis [Huh et al., 2024] suggests that different pre-trained models can represent similar objects similarly (with the same $\mathbf{z}(\mathbf{x})$), different model capacities can lead to distinct representations of a “typical” group in $\xi(\mathbf{x})$. For instance, a strong model that has learned the natural habitat of water/land birds during pre-training can encode typical samples as those with their respective backgrounds, leading to a simple, low-dimensional $\psi(\mathbf{x})$; whereas a weaker model without such knowledge have to rely on more complicated mechanisms to represent typical samples (e.g., counting), resulting in a more complex, higher-dimensional $\mathbf{w}(\mathbf{x})$.

Analogous to Dong et al. [2025], a key quantity that controls W2S gain is the similarity between the weak teacher and strong student representations, φ_T and φ_S , as formalized in Definition 1.

Definition 1 (Teacher-student similarity). Under Assumption 2, we define a similarity matrix $\Xi = \mathbf{T}^\top \mathbf{S} \in \mathbb{R}^{(p_T-1) \times (p_S-1)}$. Notice that $\|\Xi\|_F^2 \leq p_S - 1$ and $\|\Xi\|_2 \leq 1$.

Ξ measures the similarity of group features extracted by φ_T, φ_S , e.g., $\|\Xi\|_F^2 \rightarrow 0$ means $\mathbf{w}(\mathbf{x})$ and $\psi(\mathbf{x})$ are orthogonal, while $\|\Xi\|_F^2 \rightarrow p_S - 1$ means $\mathbf{w}(\mathbf{x})$ and $\psi(\mathbf{x})$ are highly aligned.

W2S fine-tuning pipeline. We consider two training sets with *i.i.d.* samples: (i) a small labeled training set $\tilde{\mathcal{S}} = \{(\tilde{\mathbf{x}}_i, \tilde{y}_i) \mid i \in [n]\} \sim \mathcal{D}(\eta_\ell)^n$ and (ii) a large unlabeled training set $\mathcal{S}_x = \{\mathbf{x}_i \mid i \in [N]\}$ from $\mathcal{S} = \{(\mathbf{x}_i, y_i) \mid i \in [N]\} \sim \mathcal{D}(\eta_u)^N$ with hidden labels, where $\eta_\ell, \eta_u \in [0, \frac{1}{2}]$. The W2S fine-tuning pipeline consists of two stages: (i) Supervised fine-tuning (SFT) of $f_T(\cdot) = \varphi_T(\cdot)^\top \boldsymbol{\theta}_T$ on $\tilde{\mathcal{S}}$ via ridgeless regression: assuming $n > d_T$,

$$\boldsymbol{\theta}_T = \underset{\boldsymbol{\theta} \in \mathbb{R}^{D_T}}{\text{argmin}} \|\boldsymbol{\theta}\|_2^2 \quad \text{s.t.} \quad \boldsymbol{\theta} \in \underset{\boldsymbol{\theta}' \in \mathbb{R}^{D_T}}{\text{argmin}} \frac{1}{n} \sum_{i=1}^n (\varphi_T(\tilde{\mathbf{x}}_i)^\top \boldsymbol{\theta}' - \tilde{y}_i)^2, \quad (1)$$

(ii) W2S fine-tuning of $f_S(\cdot) = \varphi_S(\cdot)^\top \boldsymbol{\theta}_S$ on \mathcal{S}_x labeled by f_T via ridgeless regression:

$$\boldsymbol{\theta}_S = \underset{\boldsymbol{\theta} \in \mathbb{R}^{D_S}}{\text{argmin}} \|\boldsymbol{\theta}\|_2^2 \quad \text{s.t.} \quad \boldsymbol{\theta} \in \underset{\boldsymbol{\theta}' \in \mathbb{R}^{D_S}}{\text{argmin}} \frac{1}{N} \sum_{i=1}^N (\varphi_S(\mathbf{x}_i)^\top \boldsymbol{\theta}' - f_T(\mathbf{x}_i))^2, \quad (2)$$

¹For both $\mathbf{w}(\mathbf{x})$ and $\psi(\mathbf{x})$, the first entry 1 effectively prepends the core feature $\mathbf{z}(\mathbf{x})$ in $\varphi_T(\mathbf{x})$ and $\varphi_S(\mathbf{x})$, which is essential to ensure that both teacher and student have negligible approximation error. Intuitively, pre-trained models have sufficient expressivity to learn the downstream task over population.

Remark 1 (Why ridgeless regression provides sufficient regularization?). *We note that under Assumption 2 where both φ_T and φ_S are constrained in low-dimensional subspaces, $\text{Range}(\mathbf{U}_T)$ and $\text{Range}(\mathbf{U}_S)$, ridgeless regression provides sufficient (and asymptotically optimal) regularization to avoid overfitting [Wu and Xu, 2020, Hastie et al., 2022], which is essential for W2S generalization [Burns et al., 2024]. When φ_T and φ_S concentrates in a low-dimensional subspace with a tail evenly distributed in the orthogonal complement, explicit regularization [Moniri and Hassani, 2025, Dong et al., 2025] or early stopping [Burns et al., 2024, Medvedev et al., 2025] becomes necessary to prevent the student from overfitting to noisy teacher labels. Nevertheless, analogous to Dong et al. [2025], extending our ridgeless analysis to ridge regression does not alter our key insights on spurious correlations. Therefore, we focus on the ridgeless setting for clarity of exposition.*

The generalization performance is evaluated over a test distribution $\mathcal{D}(\eta_t)$ for some $\eta_t \in [0, 1]$: with the test risk $\mathcal{R}_{\eta_t}(f) := \mathbb{E}_{(\mathbf{x}, y) \sim \mathcal{D}_{\mathbf{x}, y}(\eta_t)}[(f(\mathbf{x}) - y)^2]$, we consider the excess risk

$$\mathbf{ER}_{\eta_t}(f) := \mathcal{R}_{\eta_t}(f) - \mathcal{R}_{\eta_t}(f_*) = \mathcal{R}_{\eta_t}(f) - \sigma_y^2. \quad (3)$$

In particular, $\eta_t = \frac{1}{2}$ corresponds to the average test risk; $\eta_t = 0$ corresponds to the majority test risk; and $\eta_t = 1$ corresponds to the minority test risk.

2.2 W2S Generalization under Spurious Correlation

With the problem setup, we are ready to present our main theorems regarding the effect of spurious correlations on W2S generalization. First, to characterize the excess risks of f_T and f_S precisely, we push the problem to the proportional asymptotic limit:

Assumption 3 (Proportional asymptotic limit). *We consider $d_z, n, N \rightarrow \infty$ with $d_z/n \rightarrow \gamma_z \in (0, p_T^{-1})$ (i.e., $n > d_T$), $d_z/N \rightarrow \nu_z \in (0, p_S^{-1})$ (i.e., $N > d_S$), whereas $2 \leq p_S \leq p_T \leq p$ are fixed.*

We highlight that in practice, the unlabeled samples are typically much more affordable than the labeled ones, leading to $\nu_z \ll \gamma_z$. Now, we characterize the excess risks of the weak teacher after SFT and the strong student after W2S fine-tuning, respectively, in Theorems 1 and 2.

Theorem 1 (SFT of weak teacher (Section C.1)). *Under Assumptions 1 to 3, (1) satisfies*

$$\mathbb{E}_{\mathcal{D}(\eta_\ell)^n} [\mathbf{ER}_{\eta_t}(f_T)] \xrightarrow{\mathbb{P}} \sigma_y^2 \gamma_z \left(\underbrace{p_T}_{\mathcal{V}_T^{(0)} \text{ from variance}} + \underbrace{\frac{\|(\eta_t - \eta_\ell) \boldsymbol{\mu}_T\|_2^2}{\sigma_\xi^2}}_{\mathcal{V}_T^{(1)} \text{ from spurious correlations}} \right).$$

Theorem 2 (W2S, formally in Theorem 3). *Under Assumptions 1 to 3, (2) satisfies*

$$\mathbb{E}_{\mathcal{D}(\eta_u)^N, \mathcal{D}(\eta_\ell)^n} [\mathbf{ER}_{\eta_t}(f_S)] \xrightarrow{\mathbb{P}} \sigma_y^2 \gamma_z \left(\underbrace{p_{T \wedge S}}_{\mathcal{V}_S^{(0)} \leq \mathcal{V}_T^{(0)}} + \underbrace{\frac{\|(\eta_u - \eta_\ell) \boldsymbol{\mu}_T + (\eta_t - \eta_u) \boldsymbol{\Xi} \boldsymbol{\mu}_S\|_2^2}{\sigma_\xi^2}}_{\mathcal{V}_S^{(1)} \leq \mathcal{V}_T^{(1)} \text{ when } \eta_u = \eta_\ell} + \underbrace{\Theta(\nu_z)}_{\mathcal{E}_S \ll 1} \right),$$

where $p_{T \wedge S} = 1 + \|\boldsymbol{\Xi}\|_F^2 \in [1, p_S]$ is the effective group features dimension learned by the strong student from the weak teacher; $\mathcal{V}_S^{(0)}$ and $\mathcal{V}_T^{(0)}$ are generalization errors of f_S and f_T from variance; $\mathcal{V}_S^{(1)}$ and $\mathcal{V}_T^{(1)}$ are generalization errors of f_S and f_T induced by spurious correlations, $\eta_u, \eta_\ell \neq \eta_t$; and the higher-order term \mathcal{E}_S , formalized in Theorem 3, becomes negligible when $\nu_z \ll 1$.

As a special case, without spurious correlations ($\eta_\ell = \eta_u = \eta_t$ or $\boldsymbol{\mu}_\xi = \mathbf{0}_p$), Theorems 1 and 2 exactly recover the results in Dong et al. [2025] at the proportional asymptotic limit: $\mathbb{E}[\mathbf{ER}_{\eta_t}(f_T)] \rightarrow \sigma_y^2 \gamma_z p_T$ and $\mathbb{E}[\mathbf{ER}_{\eta_t}(f_S)] \rightarrow \sigma_y^2 \gamma_z (p_{T \wedge S} + \Theta(\nu_z))$, where with a small $\nu_z \ll 1$, the W2S gain is larger when the teacher and student representations are less aligned (*i.e.*, lower $p_{T \wedge S}$). Meanwhile, Theorems 1 and 2 together reveal novel insights regarding the effect of spurious correlations on the W2S gain: $\Delta \mathcal{R}_{\eta_t} := \mathbb{E}[\mathbf{ER}_{\eta_t}(f_T)] - \mathbb{E}[\mathbf{ER}_{\eta_t}(f_S)]$, as discussed in Remark 2.

Remark 2 (Does W2S happen under spurious correlations?). *Theorems 1 and 2 provide a mixed answer to this question conditioned on various factors, including the teacher-student similarity, the separation between groups, and the choice of η_u for given η_ℓ^2 , as summarized below:*

- (a) **W2S happens whenever $\eta_u = \eta_\ell$ and ν_z is small**, e.g., when $\|\boldsymbol{\Xi}\|_F^2 \approx 0$ and $\nu_z \ll 1$, $\Delta \mathcal{R}_{\eta_t} > 0$ is optimized at $\eta_u \approx \eta_\ell$ (Figure 1). We highlight that when $\eta_u = \eta_\ell$, in addition to the W2S gain from variance reduction $\mathcal{V}_T^{(0)} - \mathcal{V}_S^{(0)} = p_T - p_{T \wedge S} \geq 0$, **the strong student improves upon its teacher in handling spurious correlations**: $\mathcal{V}_T^{(1)} - \mathcal{V}_S^{(1)} = ((\eta_t - \eta_\ell)^2 / \sigma_\xi^2) (\|\boldsymbol{\mu}_T\|_2^2 - \|\boldsymbol{\Xi} \boldsymbol{\mu}_S\|_2^2) \geq 0$, where the gain increases as the teacher-student similarity decreases.
- (b) For fixed $\boldsymbol{\Xi}$, assume $\boldsymbol{\mu}_T \neq \boldsymbol{\Xi} \boldsymbol{\mu}_S$, when $\nu_z \ll 1$, the optimal η_u that maximizes W2S gain is $\eta_u^* = \frac{\eta_\ell \|\boldsymbol{\mu}_T\|_2^2 - (\eta_\ell + \eta_\ell) \boldsymbol{\mu}_T^\top \boldsymbol{\Xi} \boldsymbol{\mu}_S + \eta_\ell \|\boldsymbol{\Xi} \boldsymbol{\mu}_S\|_2^2}{\|\boldsymbol{\mu}_T - \boldsymbol{\Xi} \boldsymbol{\mu}_S\|_2^2}$, e.g., when $\eta_\ell = \frac{1}{2}$, $\eta_u^* = \frac{1}{2}$; when $\|\boldsymbol{\Xi} \boldsymbol{\mu}_S\|_2 \ll \|\boldsymbol{\mu}_T\|_2$, $\eta_u^* \approx \eta_\ell$; with $\|\boldsymbol{\Xi} \boldsymbol{\mu}_S\|_2 \neq 0$, η_u^* tends to increase with $\|\boldsymbol{\mu}_S\|_2^2$ and deviate from η_ℓ when $\|\boldsymbol{\mu}_S\|_2^2 \approx \|\boldsymbol{\mu}_T\|_2^2$ (Figure 2 left).
- (c) W2S gain increases as the teacher-student similarity $\|\boldsymbol{\Xi}\|_F^2$ decreases (Figure 2 right).
- (d) **W2S may not happen if $\eta_u \neq \eta_\ell$, even when $\nu_z \ll 1$ and $\|\boldsymbol{\Xi}\|_F^2 = 0$** , e.g., when $\eta_\ell = 0.4$ but $\eta_u = 0.1$, with $\|\boldsymbol{\Xi}\|_F^2 = 0$, W2S does not happen if the majority and minority groups are well separated: $\Delta \mathcal{R}_{1/2} < 0$ for any ν_z if $\|\boldsymbol{\mu}_T\|_2^2 / \sigma_\xi^2 > 12.5(p_T - 1)$. More generally, for $\|\boldsymbol{\Xi}\|_F^2 = 0$, $\mathcal{V}_S^{(1)}$ increases proportionally to $(\eta_u - \eta_\ell)^2$, and thus $\Delta \mathcal{R}_{\eta_t}$ diminishes as the gap increases.

2.3 Synthetic Experiments

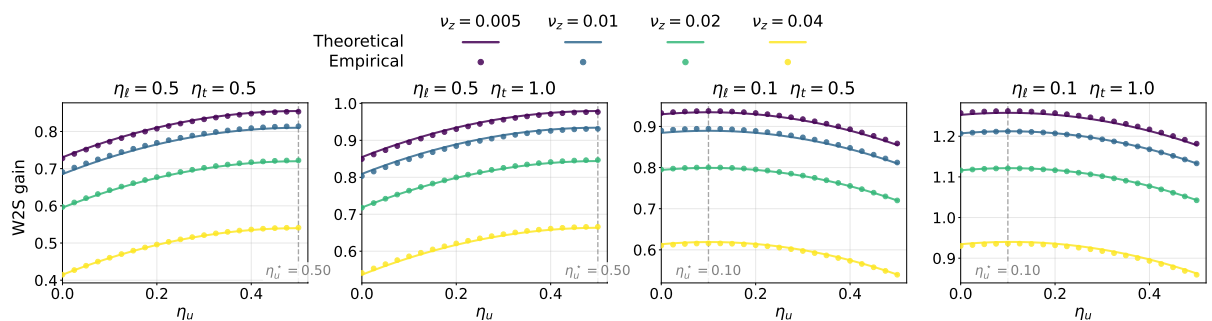


Figure 1: W2S gains across different combinations of η_ℓ and η_t . Each panel shows theoretical (solid lines) and empirical (circles) results for W2S gain as a function of η_u , across different ν_z values. Here we fix $\boldsymbol{\mu}_T$, $\boldsymbol{\mu}_S$, $\boldsymbol{\Xi}$, and d_z with $\|\boldsymbol{\mu}_T\|_2^2 = 10.0$, $\|\boldsymbol{\mu}_S\|_2^2 = 0.1$, $\|\boldsymbol{\Xi}\|_F^2 = 0.1 p_S$. Vertical dashed lines indicate the theoretical optimal η_u^* values that maximize W2S gain.

²In practice, η_ℓ is typically fixed and known (*e.g.*, given a weak teacher fine-tuned on the Waterbirds training set), while η_u can be controlled by the practitioner when collecting unlabeled data for W2S fine-tuning.

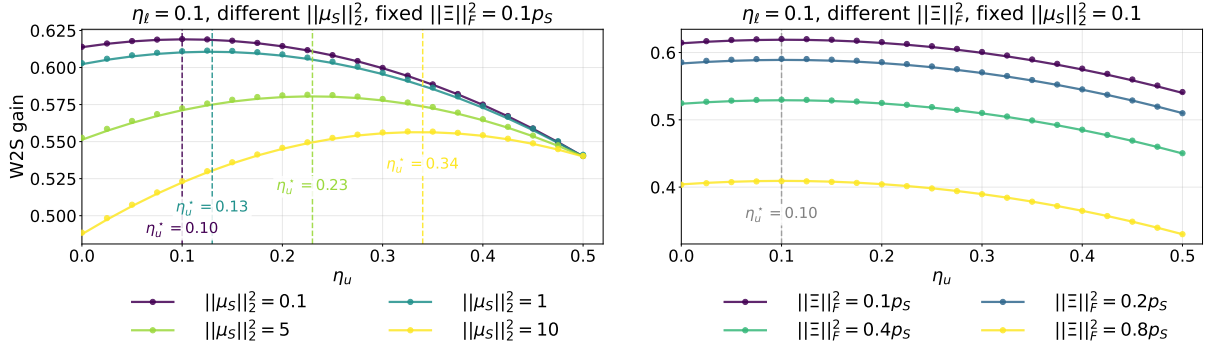


Figure 2: Impact of μ_S and Ξ on W2S gain. Both panels show theoretical (solid lines) and empirical (circles) results for W2S gain as a function of η_u . Fixed parameters: $\eta_\ell = 0.1$, $\eta_t = 0.5$, $\nu_z = 0.04$, $\|\mu_T\|_2^2 = 10.0$. Left: varying $\|\mu_S\|_2^2$ with fixed $\|\Xi\|_F^2 = 0.1ps$. Right: varying $\|\Xi\|_F^2$ with fixed $\|\mu_S\|_2^2 = 0.1$. Dashed lines indicate the theoretical optimal η_u^* values that maximize W2S gain.

Figures 1 and 2 validate the theory in Section 2.2 through synthetic Gaussian experiments, with fixed $d_z = 2048$ in all experiments. We begin by examining how varying η_u affects W2S gains under different values of η_ℓ . As shown in Figure 1, when $\|\Xi\|_F^2$ is small (a distinct teacher-student pair), W2S gains are maximized at $\eta_u \approx \eta_\ell$ for both balanced ($\eta_\ell = 0.5$) and highly spurious ($\eta_\ell = 0.1$) unlabeled data. This holds for both the average test risk and the minority test risk, consistent with Remark 2(a). Moreover, the magnitude of the W2S gain decreases as ν_z increases, reflecting the role of \mathcal{E}_S in Theorem 2. Figure 2 left shows that as $\|\mu_S\|_2^2$ increases so that $\|\Xi\mu_S\|_2^2$ becomes non-negligible compared to $\|\mu_T\|_2^2$, the optimal value η_u^* gradually shifts away from η_ℓ . This indicates that in some special cases η_u^* may not lie near η_ℓ , consistent with Remark 2(b). Figure 2 right illustrates that the W2S gain decreases as the teacher-student similarity $\|\Xi\|_F^2$ increases, consistent with Remark 2(c).

3 Real-World Evaluation

Now we extend our theoretical understanding of W2S under spurious correlation to real-world tasks. We first leverage the theoretical framework to interpret our findings on how spurious correlations affect W2S performance across real-world benchmarks.

3.1 Model and Dataset Setup

Pre-trained models. Our weak teachers and strong students are drawn from a diverse set of pre-trained vision backbones that differ in architecture and training paradigm. Specifically, we consider ResNet-18 (ResNet18) [He et al., 2016], CLIP ViT-B/32 (Clipb32) [Radford et al., 2021], ConvNeXt-L (ConvNeXt) [Liu et al., 2022], DINOv2 ViT-L/14 (DINOv2) [Oquab et al., 2023], and MAE ViT-B/16 (MAE) [He et al., 2022]. For each experiment on a given dataset, we include all teacher—student pairs whose relative strength (measured by accuracy) remains stable when we vary parameters including η_ℓ , η_u , N , or n . We freeze all backbone parameters, view the pre-trained feature for the teacher and the student as φ_T and φ_S , and only finetune the classification head.

Datasets. From both theoretical and practical perspectives, effective W2S requires that the pre-trained weak teacher and strong student have learned feature representations that are useful for the downstream task. Therefore, we evaluate W2S performance on widely used spurious correlation benchmarks that are relatively close to the pre-training distribution. These include Waterbirds [Sagawa et al., 2020], BFFHQ [Lee et al., 2021], and ImageNet-9 [Xiao et al., 2020], which contain spurious correlations between background and bird labels, age and gender labels, and background and object labels, respectively. We further provide a self-generated dataset, BG-COCO, by creating spurious correlations between cats/dogs from COCO [Lin et al., 2014] and indoor/outdoor scenes from Places [Zhou et al., 2017]. We note that in all four datasets, the spurious correlation arises from highly imbalanced group proportions between the majority and minority groups. We denote the minority group proportion in the original training set of each dataset as η_o , which equals 0.05, 0.005, 0, and 0.05 for Waterbirds, BFFHQ, ImageNet-9, and BG-COCO, respectively. Detailed configurations of the dataset splits are provided in Appendix D.1.

3.2 Interpreting W2S under Spurious Correlations

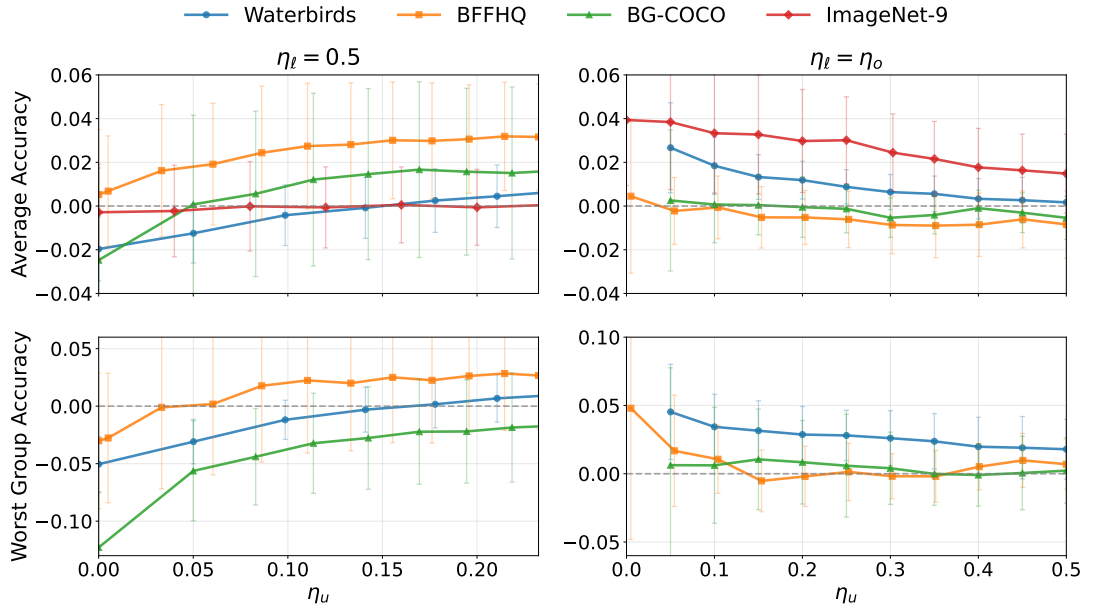


Figure 3: Average W2S gain across all teacher-student pairs as a function of η_u on all four datasets. Top row: average accuracy; bottom row: worst group accuracy. Left column fixes $\eta_t = 0.5$; right column fixes $\eta_t = \eta_o$. For $\eta_t = 0.5$, curves are plotted over a shared η_u interval aligned across datasets (bounded by minority group sample availability) to enable direct comparability. For $\eta_t = \eta_o$, each dataset is plotted from its own η_o (0.05, 0.005, 0.05, and 0 for Waterbirds, BFFHQ, BG-COCO, and ImageNet-9, respectively) up to 0.5. ImageNet-9 does not have a clearly defined worst group and is therefore omitted from the bottom panels.

We investigate how the proportion of the minority group in the unlabeled data affects W2S performance when the labeled data are either group-balanced or group-imbalanced. Specifically, we fix $\eta_t = 0.5$ and $\eta_t = \eta_o$, respectively, and vary η_u while recording the change in W2S gain.³

³For classification tasks, W2S gain refers to the improvement in test accuracy achieved by the strong student after W2S fine-tuning over its weak teacher.

Figure 3 presents the average W2S gain across all teacher–student pairs on all four datasets. More comprehensive results are provided in Appendix D.2.

Our results show that, for both average accuracy ($\eta_t = 0.5$) and worst group accuracy ($\eta_t = 1$), increasing the minority proportion in the unlabeled data improves W2S performance when the weak teacher is free of spurious correlation ($\eta_\ell = 0.5$). Moreover, when the weak teacher itself encodes spurious correlation ($\eta_\ell = \eta_o$), the W2S gain is consistently positive across all four datasets at $\eta_u = \eta_o$, but surprisingly decreases for more balanced data as η_u increases from η_o to 0.5. Overall, W2S gain is negatively affected as the gap between η_u and η_ℓ increases. These observations echo our theory and synthetic experiments (see Theorems 1 and 2, Remark 2, and Figure 1), showing that our theoretical findings on regression extends naturally to broader, real-world classification problems.

4 Enhanced-W2S Method

Inspired by the theory and observations in Sections 2 and 3, we introduce a simple retraining method based on student confidence and generalized cross-entropy to strengthen W2S under spurious correlations. We show that this approach remarkably outperforms vanilla W2S across multiple datasets and large pre-trained backbones, without requiring any group annotations.

Method. Both our theoretical results and empirical findings indicate that W2S gain is noticeably reduced when there is a large discrepancy between the minority proportions of the unlabeled data and the labeled data. Therefore, we propose a simple method that requires no group label annotations and is capable of improving W2S gain in two particularly important settings: one where the labeled data are heavily affected by spurious correlation while the unlabeled data are free of it ($\eta_\ell = \eta_o, \eta_u = 0.5$), and the other where the unlabeled data suffer from spurious correlation while the labeled data are balanced ($\eta_\ell = 0.5, \eta_u = \eta_o$).

Formally, let the unlabeled data be $\hat{\mathcal{S}} = \{(\mathbf{x}_i, \hat{y}_i) \mid i \in [N]\}$, where \hat{y}_i is the pseudolabel given by the weak teacher on $\mathbf{x}_i \in \mathcal{S}_x$. Our method enhances W2S gain by retraining the strong student after W2S fine-tuning, based on two components: (i) selecting a fraction $p \in (0, 1]$ of $\hat{\mathcal{S}}$ consisting of the samples with the highest student confidence (equivalently, the lowest entropy), and (ii) applying the generalized cross-entropy (GCE) loss [Zhang and Sabuncu, 2018] with parameter $q \in (0, 1]$ to each $(\mathbf{x}_i, \hat{y}_i)$ in this subset:

$$\mathcal{L}_{\text{GCE}}(\mathbf{x}_i, \hat{y}_i; q) = \frac{1 - \mathbf{p}_{\hat{y}_i}(\mathbf{x}_i)^q}{q},$$

where $\mathbf{p}_{\hat{y}_i}(\mathbf{x}_i)$ is the softmax probability that the student assigns to the pseudolabel \hat{y}_i for \mathbf{x}_i .

In both settings ($\eta_\ell = \eta_o, \eta_u = 0.5$ and $\eta_\ell = 0.5, \eta_u = \eta_o$), selecting a high-confidence subset of the student’s predictions filters for samples where all relevant features are clearly expressed and effectively used during prediction, thus preventing the strong student from over-relying on any single (potentially spurious) feature. Moreover, unlike the CE loss which imposes overly strong penalties on high-confidence but incorrect pseudolabels, applying the GCE loss to the selected subset mitigates the negative impact of pseudolabel noise from the weak teacher.⁴

⁴In our Enhanced-W2S method, the role of GCE loss is analogous to its original use in Zhang and Sabuncu

More importantly, for the case $\eta_\ell = \eta_o, \eta_u = 0.5$, confidence-based selection further provides a crucial benefit. As shown in Appendix D.3, the high-confidence subset tends to filter out a larger fraction of minority samples to effectively reduce the new η_u during retraining. This observation aligns with our theoretical prediction that when $\eta_\ell = \eta_o$, decreasing η_u from 0.5 leads to improved W2S gain.

Dataset	η_ℓ	η_u	Teacher–Student pair									
			DINOv2		DINOv2		DINOv2		DINOv2		ConvNeXt	
			ConvNeXt	Clipb32	ResNet18	MAE	Clipb32	ResNet18	MAE	Clipb32	ResNet18	MAE
Waterbirds	0.5	η_o	6.60	11.29	7.34	16.68	3.79	2.05	6.28	—	2.07	0.77
	η_o	0.5	7.19	13.86	11.73	11.62	2.85	2.02	4.33	—	1.32	14.54
BFFHQ	0.5	η_o	6.85	2.75	8.42	4.93	4.05	—	—	6.54	5.12	—
	η_o	0.5	3.92	8.53	2.02	4.56	2.09	—	—	2.06	-1.37	—
BG-COCO	0.5	η_o	5.38	13.40	12.88	24.01	9.82	6.49	15.25	3.39	12.43	2.05
	η_o	0.5	10.21	16.99	12.25	-3.52	3.41	1.21	-3.07	3.48	0.31	3.70
ImageNet-9	0.5	η_o	—	6.03	7.45	24.11	4.74	5.30	18.49	4.22	21.73	17.98
	η_o	0.5	—	8.21	11.28	22.00	3.77	1.81	10.50	4.51	23.24	15.76

Table 1: Relative improvement of Enhanced-W2S over vanilla W2S (%, measured by average accuracy) across all datasets and teacher–student pairs. Each entry reports the mean improvement over all N, n combinations. For each model pair in the table header, the assignment of weak teacher and strong student depends on the dataset. We report for each dataset only those model pairs whose relative strength relationship remains consistent across different (η_ℓ, η_u) settings within that dataset.

Main results. We evaluate our Enhanced-W2S method across all four datasets. Table 1 reports the relative improvement of Enhanced-W2S over vanilla W2S for each teacher–student pair. Figure 4 further visualizes the performance of Enhanced-W2S versus vanilla W2S for a representative model pair. Overall, for both average accuracy and worst group accuracy, Enhanced-W2S achieves consistent and substantial improvements over vanilla W2S under both (η_ℓ, η_u) settings. Specifically, Table 1 shows that 67 out of 70 model pairs exhibit a positive gain (measured by average accuracy), with the mean relative improvements across all pairs reaching 7.02% (Waterbirds), 4.32% (BFFHQ), 7.50% (BG-COCO), and 11.73% (ImageNet-9). In addition, the relative improvement of Enhanced-W2S in terms of worst group accuracy across all pairs is 21.14% (Waterbirds), 3.81% (BFFHQ), and 7.73% (BG-COCO). Further details are provided in Appendix D.3.

Ablation study. We conduct controlled ablations to examine the contribution of the two key components of our Enhanced-W2S methods, namely the use of the GCE loss and confidence-based selection. Specifically, we conduct two separate ablations: (i) replacing the GCE loss with the standard CE loss, and (ii) replacing confidence-based selection with using the full unlabeled dataset. We then retrain the model under each variant and compare the results with the original Enhanced-W2S method. Table 2 shows that under both (η_ℓ, η_u) settings, the GCE loss and confidence-based selection each play a positive role in improving W2S gain. When

[2018] for handling noisy labels. Different from the setting studied in Nam et al. [2020], where GCE loss on ground-truth labeled datasets with spurious correlations was observed to amplify bias, in our method GCE loss is applied to a pseudolabeled dataset restricted to a high-confidence subset, and thus serves a fundamentally different role.

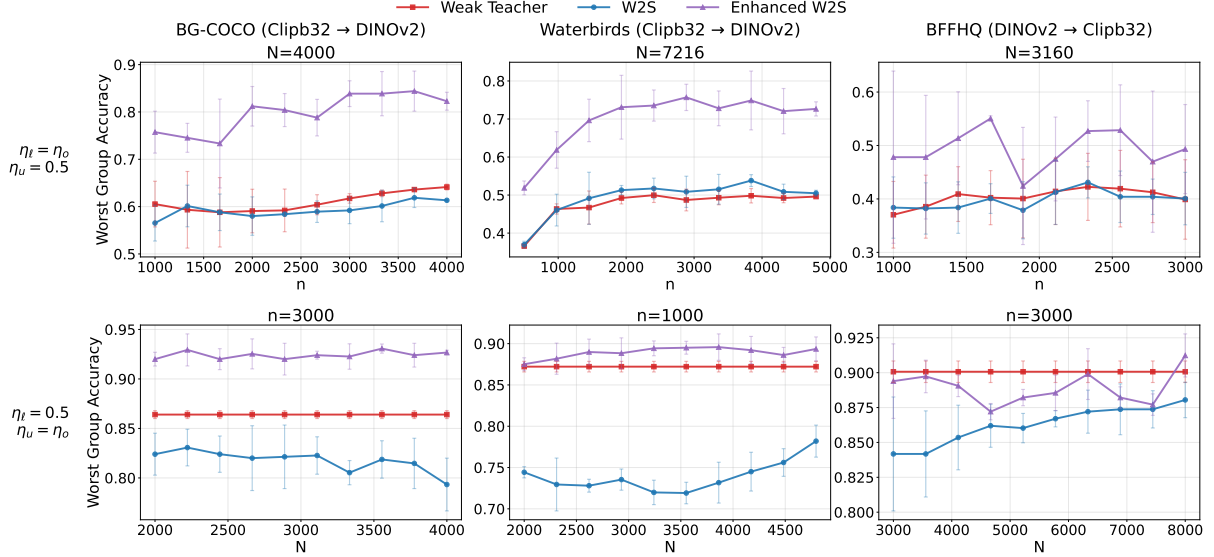


Figure 4: Comparison of Enhanced-W2S and original W2S for the (Clipb32, DINov2) pair on BG-COCO, Waterbirds, and BFFHQ. Top row: worst group accuracy with $\eta_\ell = \eta_o$, $\eta_u = 0.5$ (fixed N , varying n). Bottom row: worst group accuracy with $\eta_\ell = 0.5$, $\eta_u = \eta_o$ (fixed n , varying N).

Comparison	Metric ($\times 10^{-2}$)	Waterbirds		BFFHQ		BG-COCO		ImageNet-9	
		(η_ℓ, η_u)		(η_ℓ, η_u)		(η_ℓ, η_u)		(η_ℓ, η_u)	
		$(0.5, \eta_o)$	$(\eta_o, 0.5)$						
Enhanced W2S – Enhanced W2S ($q \rightarrow 0$)	Average	3.27	1.00	3.51	0.46	3.41	0.52	1.00	0.51
	Worst	5.15	2.39	4.34	1.90	3.79	1.46	—	—
Enhanced W2S – Enhanced W2S ($p = 1$)	Average	2.79	4.84	2.77	2.69	4.97	3.37	4.51	5.08
	Worst	3.57	8.58	2.75	3.73	6.26	5.44	—	—

Table 2: Ablation across four datasets: improvements of Enhanced-W2S over two baselines, using only the CE loss (i.e., the $q \rightarrow 0$ limit of GCE) and using all unlabeled data ($p = 1$), in terms of either average accuracy or worst group accuracy. For each dataset, improvements are computed as the mean across all model pairs whose relative strength relationship remains consistent under different (η_ℓ, η_u) settings. ImageNet-9 has no well-defined worst group, so those entries are omitted.

$\eta_\ell = \eta_o$, $\eta_u = 0.5$, the impact of using CE loss is consistently smaller than that of using the full unlabeled dataset; whereas under $\eta_\ell = 0.5$, $\eta_u = \eta_o$, the effects of the two ablations are more comparable. This suggests that filtering out minority group samples via high-confidence selection plays a more critical role in the former setting, while in the latter setting the contributions of GCE and high-confidence selection are comparable.

5 Conclusions and Discussions

In this work, we start with a theoretical framework that studies W2S generalization under spurious correlations induced by group imbalance. This framework precisely reveals how

different key factors (e.g., the proportions of minority groups in labeled and unlabeled data, and the teacher-student similarity) affect the W2S gain. Second, we validated the theoretical predictions through extensive synthetic experiments and diverse real-world tasks. Third, we proposed Enhanced-W2S, a confidence-based retraining algorithm that does not require any group labels and substantially improves W2S gains when the labeled or unlabeled data are highly group-imbalanced. Finally, we demonstrated the effectiveness of this approach across assorted real-world datasets.

In addition, it is important to emphasize that spurious correlations in W2S constitute a critical issue that deserves closer attention. Beyond standard benchmarks, such correlations can pose substantial risks: in socially sensitive domains they may reflect demographic biases, and in safety-critical applications they can degrade reliability under rare but high-stakes conditions. While our experiments focus on public computer vision benchmarks, the mechanisms we analyze are broadly relevant. Our algorithm provides the first attempt to improve W2S in this setting, and we hope this work will inspire further efforts toward more reliable and efficient W2S methods.

Acknowledgments

The authors would like to thank Jason D. Lee and Denny Wu for insightful discussions. YD acknowledges support of the NYU Courant Instructorship. QL acknowledges support of NSF DMS-2523382 and DOE Office of Science under Award #DE-SC0024721.

References

Josh Achiam, Steven Adler, Sandhini Agarwal, Lama Ahmad, Ilge Akkaya, Florencia Leoni Aleman, Diogo Almeida, Janko Altenschmidt, Sam Altman, Shyamal Anadkat, et al. GPT-4 technical report. *arXiv preprint arXiv:2303.08774*, 2023.

Armen Aghajanyan, Sonal Gupta, and Luke Zettlemoyer. Intrinsic dimensionality explains the effectiveness of language model fine-tuning. In *Proceedings of the 59th Annual Meeting of the Association for Computational Linguistics and the 11th International Joint Conference on Natural Language Processing (Volume 1: Long Papers)*, pages 7319–7328, 2021.

Martin Arjovsky, Léon Bottou, Ishaan Gulrajani, and David Lopez-Paz. Invariant risk minimization. *arXiv preprint arXiv:1907.02893*, 2019.

Tom Brown, Benjamin Mann, Nick Ryder, Melanie Subbiah, Jared D Kaplan, Prafulla Dhariwal, Arvind Neelakantan, Pranav Shyam, Girish Sastry, Amanda Askell, et al. Language models are few-shot learners. *Advances in neural information processing systems*, 33:1877–1901, 2020.

Collin Burns, Pavel Izmailov, Jan Hendrik Kirchner, Bowen Baker, Leo Gao, Leopold Aschenbrenner, Yining Chen, Adrien Ecoffet, Manas Joglekar, Jan Leike, et al. Weak-to-strong generalization: eliciting strong capabilities with weak supervision. In *Proceedings of the 41st International Conference on Machine Learning*, pages 4971–5012, 2024.

Ilias Chalkidis, Tommaso Pasini, Sheng Zhang, Letizia Tomada, Sebastian Felix Schwemer, and Anders Søgaard. Fairlex: A multilingual benchmark for evaluating fairness in legal text processing. *arXiv preprint arXiv:2203.07228*, 2022.

Moses Charikar, Chirag Pabbaraju, and Kirankumar Shiragur. Quantifying the gain in weak-to-strong generalization. *Advances in neural information processing systems*, 37:126474–126499, 2024.

Yihe Deng, Yu Yang, Baharan Mirzasoleiman, and Quanquan Gu. Robust learning with progressive data expansion against spurious correlation. *Advances in neural information processing systems*, 36:1390–1402, 2023.

Yijun Dong, Kevin Miller, Qi Lei, and Rachel Ward. Cluster-aware semi-supervised learning: relational knowledge distillation provably learns clustering. *Advances in Neural Information Processing Systems*, 36, 2024.

Yijun Dong, Yicheng Li, Yunai Li, Jason D Lee, and Qi Lei. Discrepancies are virtue: Weak-to-strong generalization through lens of intrinsic dimension. In *Forty-second International Conference on Machine Learning*. PMLR, 2025.

Shashwat Goel, Joschka Strüber, Ilze Amanda Auzina, Karuna K Chandra, Ponnurangam Kumaraguru, Douwe Kiela, Ameya Prabhu, Matthias Bethge, and Jonas Geiping. Great models think alike and this undermines ai oversight. In *Forty-second International Conference on Machine Learning*, 2025.

Jianyuan Guo, Hanting Chen, Chengcheng Wang, Kai Han, Chang Xu, and Yunhe Wang. Vision superalignment: Weak-to-strong generalization for vision foundation models. *arXiv preprint arXiv:2402.03749*, 2024.

Yue Guo and Yi Yang. Improving weak-to-strong generalization with reliability-aware alignment. *arXiv preprint arXiv:2406.19032*, 2024.

Alpana K Gupta, Mausumi Bharadwaj, and Ravi Mehrotra. Skin cancer concerns in people of color: risk factors and prevention. *Asian Pacific journal of cancer prevention: APJCP*, 17(12):5257, 2016.

Yujin Han and Difan Zou. Improving group robustness on spurious correlation requires preciser group inference. *arXiv preprint arXiv:2404.13815*, 2024.

Trevor Hastie, Andrea Montanari, Saharon Rosset, and Ryan J Tibshirani. Surprises in high-dimensional ridgeless least squares interpolation. *Annals of statistics*, 50(2):949, 2022.

Kaiming He, Xiangyu Zhang, Shaoqing Ren, and Jian Sun. Deep residual learning for image recognition. In *Proceedings of the IEEE conference on computer vision and pattern recognition*, pages 770–778, 2016.

Kaiming He, Xinlei Chen, Saining Xie, Yanghao Li, Piotr Dollár, and Ross Girshick. Masked autoencoders are scalable vision learners. In *Proceedings of the IEEE/CVF conference on computer vision and pattern recognition*, pages 16000–16009, 2022.

Geoffrey Hinton, Oriol Vinyals, and Jeff Dean. Distilling the knowledge in a neural network. *arXiv preprint arXiv:1503.02531*, 2015.

Minyoung Huh, Brian Cheung, Tongzhou Wang, and Phillip Isola. The platonic representation hypothesis. *arXiv preprint arXiv:2405.07987*, 2024.

Muhammed Emrullah Ildiz, Halil Alperen Gozeten, Ege Onur Taga, Marco Mondelli, and Samet Oymak. High-dimensional analysis of knowledge distillation: Weak-to-strong generalization and scaling laws. In *ICLR*, 2025.

Arthur Jacot, Franck Gabriel, and Clément Hongler. Neural tangent kernel: Convergence and generalization in neural networks. *Advances in neural information processing systems*, 31, 2018.

Patrik Kenfack, Ulrich Aïvodji, and Samira Ebrahimi Kahou. Adaptive group robust ensemble knowledge distillation. *arXiv preprint arXiv:2411.14984*, 2024.

David Krueger, Ethan Caballero, Joern-Henrik Jacobsen, Amy Zhang, Jonathan Binas, Dinghuai Zhang, Remi Le Priol, and Aaron Courville. Out-of-distribution generalization via risk extrapolation (rex). In *International conference on machine learning*, pages 5815–5826. PMLR, 2021.

Tyler LaBonte, Vidya Muthukumar, and Abhishek Kumar. Towards last-layer retraining for group robustness with fewer annotations. *Advances in Neural Information Processing Systems*, 36, 2024.

Hunter Lang, David Sontag, and Aravindan Vijayaraghavan. Theoretical analysis of weak-to-strong generalization. In *The Thirty-eighth Annual Conference on Neural Information Processing Systems*, 2024.

Beatrice Laurent and Pascal Massart. Adaptive estimation of a quadratic functional by model selection. *Annals of statistics*, pages 1302–1338, 2000.

Jiwoon Lee and Jaeho Lee. Debiased distillation by transplanting the last layer. *arXiv preprint arXiv:2302.11187*, 2023.

Jungsoo Lee, Eungyeup Kim, Juyoung Lee, Jihyeon Lee, and Jaegul Choo. Learning debiased representation via disentangled feature augmentation. *Advances in Neural Information Processing Systems*, 34:25123–25133, 2021.

Jan Leike and Ilya Sutskever. Introducing superalignment, July 2023. Accessed: 2025-09-24.

Ming Li, Yong Zhang, Shuai He, Zhitao Li, Hongyu Zhao, Jianzong Wang, Ning Cheng, and Tianyi Zhou. Superfiltering: Weak-to-strong data filtering for fast instruction-tuning. In *Proceedings of the 62nd Annual Meeting of the Association for Computational Linguistics (Volume 1: Long Papers)*, pages 14255–14273, 2024.

Tsung-Yi Lin, Michael Maire, Serge Belongie, James Hays, Pietro Perona, Deva Ramanan, Piotr Dollár, and C Lawrence Zitnick. Microsoft coco: Common objects in context. In *European conference on computer vision*, pages 740–755. Springer, 2014.

Chenruo Liu, Hongjun Liu, Zeyu Lai, Yiqiu Shen, Chen Zhao, and Qi Lei. Superclass-guided representation disentanglement for spurious correlation mitigation. *arXiv preprint arXiv:2508.08570*, 2025a.

Chenruo Liu, Kenan Tang, Yao Qin, and Qi Lei. Bridging distribution shift and ai safety: Conceptual and methodological synergies. *arXiv preprint arXiv:2505.22829*, 2025b.

Evan Z Liu, Behzad Haghgoo, Annie S Chen, Aditi Raghunathan, Pang Wei Koh, Shiori Sagawa, Percy Liang, and Chelsea Finn. Just train twice: Improving group robustness without training group information. In *International Conference on Machine Learning*, pages 6781–6792. PMLR, 2021.

Mingyu Liu, Ekim Yurtsever, Jonathan Fossaert, Xingcheng Zhou, Walter Zimmer, Yuning Cui, Bare Luka Zagar, and Alois C Knoll. A survey on autonomous driving datasets: Statistics, annotation quality, and a future outlook. *IEEE Transactions on Intelligent Vehicles*, 2024.

Yuejiang Liu and Alexandre Alahi. Co-supervised learning: Improving weak-to-strong generalization with hierarchical mixture of experts. *arXiv preprint arXiv:2402.15505*, 2024.

Zhuang Liu, Hanzi Mao, Chao-Yuan Wu, Christoph Feichtenhofer, Trevor Darrell, and Saining Xie. A convnet for the 2020s. In *Proceedings of the IEEE/CVF conference on computer vision and pattern recognition*, pages 11976–11986, 2022.

Michal Lukasik, Srinadh Bhojanapalli, Aditya Krishna Menon, and Sanjiv Kumar. Teacher’s pet: understanding and mitigating biases in distillation. *arXiv preprint arXiv:2106.10494*, 2021.

Sadhika Malladi, Alexander Wettig, Dingli Yu, Danqi Chen, and Sanjeev Arora. A kernel-based view of language model fine-tuning. In *International Conference on Machine Learning*, pages 23610–23641. PMLR, 2023.

Marko Medvedev, Kaifeng Lyu, Dingli Yu, Sanjeev Arora, Zhiyuan Li, and Nathan Srebro. Weak-to-strong generalization even in random feature networks, provably. In *Forty-second International Conference on Machine Learning*. PMLR, 2025.

Behrad Moniri and Hamed Hassani. On the mechanisms of weak-to-strong generalization: A theoretical perspective. *arXiv preprint arXiv:2505.18346*, 2025.

Abhijeet Mulgund and Chirag Pabbaraju. Relating misfit to gain in weak-to-strong generalization beyond the squared loss. In *Forty-second International Conference on Machine Learning*, 2025.

Vaishnavh Nagarajan, Aditya K Menon, Srinadh Bhojanapalli, Hossein Mobahi, and Sanjiv Kumar. On student-teacher deviations in distillation: does it pay to disobey? *Advances in Neural Information Processing Systems*, 36:5961–6000, 2023.

Junhyun Nam, Hyuntak Cha, Sungsoo Ahn, Jaeho Lee, and Jinwoo Shin. Learning from failure: De-biasing classifier from biased classifier. *Advances in Neural Information Processing Systems*, 33:20673–20684, 2020.

Junsoo Oh, Jerry Song, and Chulhee Yun. From linear to nonlinear: Provable weak-to-strong generalization through feature learning. In *High-dimensional Learning Dynamics 2025*, 2025.

Utkarsh Ojha, Yuheng Li, Anirudh Sundara Rajan, Yingyu Liang, and Yong Jae Lee. What knowledge gets distilled in knowledge distillation? *Advances in Neural Information Processing Systems*, 36:11037–11048, 2023.

Maxime Oquab, Timothée Darcet, Théo Moutakanni, Huy Vo, Marc Szafraniec, Vasil Khalidov, Pierre Fernandez, Daniel Haziza, Francisco Massa, Alaaeldin El-Nouby, et al. Dinov2: Learning robust visual features without supervision. *arXiv preprint arXiv:2304.07193*, 2023.

Hoang Phan, Andrew Gordon Wilson, and Qi Lei. Controllable prompt tuning for balancing group distributional robustness. *arXiv preprint arXiv:2403.02695*, 2024.

Mary Phuong and Christoph Lampert. Towards understanding knowledge distillation. In *International conference on machine learning*, pages 5142–5151. PMLR, 2019.

Aahlad Puli, Lily H Zhang, Eric K Oermann, and Rajesh Ranganath. Out-of-distribution generalization in the presence of nuisance-induced spurious correlations. *arXiv preprint arXiv:2107.00520*, 2021.

Alec Radford, Jong Wook Kim, Chris Hallacy, Aditya Ramesh, Gabriel Goh, Sandhini Agarwal, Girish Sastry, Amanda Askell, Pamela Mishkin, Jack Clark, et al. Learning transferable visual models from natural language supervision. In *International conference on machine learning*, pages 8748–8763. PmLR, 2021.

Shiori Sagawa, Pang Wei Koh, Tatsunori B Hashimoto, and Percy Liang. Distributionally robust neural networks. In *International Conference on Learning Representations*, 2020.

Changho Shin, John Cooper, and Frederic Sala. Weak-to-strong generalization through the data-centric lens. In *The Thirteenth International Conference on Learning Representations*, 2025.

Seamus Somerstep, Felipe Maia Polo, Moulinath Banerjee, Yaakov Ritov, Mikhail Yurochkin, and Yuekai Sun. A statistical framework for weak-to-strong generalization. In *ICML 2024 Next Generation of AI Safety Workshop*, 2024.

Samuel Stanton, Pavel Izmailov, Polina Kirichenko, Alexander A Alemi, and Andrew G Wilson. Does knowledge distillation really work? *Advances in Neural Information Processing Systems*, 34:6906–6919, 2021.

Joel A Tropp. User-friendly tail bounds for sums of random matrices. *Foundations of computational mathematics*, 12(4):389–434, 2012.

Konstantinos Vilouras, Xiao Liu, Pedro Sanchez, Alison Q O’Neil, and Sotirios A Tsaftaris. Group distributionally robust knowledge distillation. In *International Workshop on Machine Learning in Medical Imaging*, pages 234–242. Springer, 2023.

Serena Wang, Harikrishna Narasimhan, Yichen Zhou, Sara Hooker, Michal Lukasik, and Aditya Krishna Menon. Robust distillation for worst-class performance: on the interplay between teacher and student objectives. In *Uncertainty in Artificial Intelligence*, pages 2237–2247. PMLR, 2023.

Tao Wen, Zihan Wang, Quan Zhang, and Qi Lei. Elastic representation: Mitigating spurious correlations for group robustness. *arXiv preprint arXiv:2502.09850*, 2025.

David Xing Wu and Anant Sahai. Provable weak-to-strong generalization via benign overfitting. In *The Thirteenth International Conference on Learning Representations*, 2025.

Denny Wu and Ji Xu. On the optimal weighted ℓ_2 regularization in overparameterized linear regression. *Advances in Neural Information Processing Systems*, 33:10112–10123, 2020.

Kai Xiao, Logan Engstrom, Andrew Ilyas, and Aleksander Madry. Noise or signal: The role of image backgrounds in object recognition. *ArXiv preprint arXiv:2006.09994*, 2020.

Gengze Xu, Wei Yao, Ziqiao Wang, and Yong Liu. On the emergence of weak-to-strong generalization: A bias-variance perspective. *arXiv preprint arXiv:2505.24313*, 2025.

Yihao Xue, Jiping Li, and Baharan Mirzasoleiman. Representations shape weak-to-strong generalization: Theoretical insights and empirical predictions. In *Forty-second International Conference on Machine Learning*, 2025.

Wenkai Yang, Shiqi Shen, Guangyao Shen, Wei Yao, Yong Liu, Gong Zhi, Yankai Lin, and Ji-Rong Wen. Super (ficial)-alignment: Strong models may deceive weak models in weak-to-strong generalization. In *The Thirteenth International Conference on Learning Representations*, 2025.

Yuqing Yang, Yan Ma, and Pengfei Liu. Weak-to-strong reasoning. In *Findings of the Association for Computational Linguistics: EMNLP 2024*, pages 8350–8367, 2024.

Wei Yao, Wenkai Yang, Ziqiao Wang, Yankai Lin, and Yong Liu. Understanding the capabilities and limitations of weak-to-strong generalization. In *Scaling Self-Improving Foundation Models without Human Supervision*, 2025.

Sriram Yenamandra, Pratik Ramesh, Viraj Prabhu, and Judy Hoffman. Facts: First amplify correlations and then slice to discover bias. In *Proceedings of the IEEE/CVF International Conference on Computer Vision*, pages 4794–4804, 2023.

John R Zech, Marcus A Badgeley, Manway Liu, Anthony B Costa, Joseph J Titano, and Eric Karl Oermann. Variable generalization performance of a deep learning model to detect pneumonia in chest radiographs: a cross-sectional study. *PLoS medicine*, 15(11):e1002683, 2018.

Jingzhao Zhang, Aditya Menon, Andreas Veit, Srinadh Bhojanapalli, Sanjiv Kumar, and Suvrit Sra. Coping with label shift via distributionally robust optimisation. *arXiv preprint arXiv:2010.12230*, 2020.

Michael Zhang, Nimit S Sohoni, Hongyang R Zhang, Chelsea Finn, and Christopher Ré. Correct-n-contrast: A contrastive approach for improving robustness to spurious correlations. *arXiv preprint arXiv:2203.01517*, 2022.

Zhilu Zhang and Mert Sabuncu. Generalized cross entropy loss for training deep neural networks with noisy labels. *Advances in neural information processing systems*, 31, 2018.

Bolei Zhou, Agata Lapedriza, Aditya Khosla, Aude Oliva, and Antonio Torralba. Places: A 10 million image database for scene recognition. *IEEE Transactions on Pattern Analysis and Machine Intelligence*, 2017.

Appendices

A Usage of Large Language Models	19
B Additional Notations	19
C Proofs for Section 2.2	19
C.1 SFT of Weak Teacher	20
C.2 W2S Fine-tuning of Strong Student	25
D Additional Experimental Details	30
D.1 Dataset Statistics	30
D.2 Results for Interpreting W2S under Spurious Correlations	32
D.3 Results for Enhanced W2S	33

A Usage of Large Language Models

Large language models were used in a limited manner to (i) search for related literature, (ii) check grammar/phrasing, and (iii) make stylistic adjustments (*e.g.*, generating `tikz` decoration of equations, tables, and figures).

B Additional Notations

For any $n \in \mathbb{N}$, let $[n] = \{1, 2, \dots, n\}$. \mathbf{e}_i is the i -th canonical basis of a conformable dimension. We adapt the standard big-O notations for functions of multiple variables: for two functions $f, g : \mathbb{N}^k \rightarrow \mathbb{R}_{\geq 0}$, $f(\mathbf{n}) = O(g(\mathbf{n}))$ means that there exists a constant $C > 0$ such that $f(\mathbf{n}) \leq Cg(\mathbf{n})$ for all $\mathbf{n} \in \mathbb{N}^k$; $f(\mathbf{n}) = \Omega(g(\mathbf{n}))$ means that there exists a constant $c > 0$ such that $f(\mathbf{n}) \geq cg(\mathbf{n})$ for all $\mathbf{n} \in \mathbb{N}^k$; $f(\mathbf{n}) = \Theta(g(\mathbf{n}))$ means that $f(\mathbf{n}) = O(g(\mathbf{n}))$ and $f(\mathbf{n}) = \Omega(g(\mathbf{n}))$; $f(\mathbf{n}) = o(g(\mathbf{n}))$ means that $\lim_{\min_i n_i \rightarrow \infty} f(\mathbf{n})/g(\mathbf{n}) = 0$. For a scalar quantity $f(n) \geq 0$ depending on $n \in \mathbb{N}$, $f(n) = O_{\mathbb{P}}(g(n))$ means that for any $\delta \in (0, 1)$, there exists a constant $C(\delta) > 0$, independent of n , and a natural number $N(\delta) \in \mathbb{N}$ such that $\Pr[f(n) \leq C(\delta)g(n)] \geq 1 - \delta$ for all $n \geq N(\delta)$.

C Proofs for Section 2.2

We first observe that when $n > d_T$, (1) can be equivalently written as $\boldsymbol{\theta}_T = \mathbf{U}_T \boldsymbol{\beta}_T$ where

$$\boldsymbol{\beta}_T = \underset{\boldsymbol{\beta} \in \mathbb{R}^{d_T}}{\operatorname{argmin}} \frac{1}{n} \sum_{i=1}^n (\phi_T(\tilde{\mathbf{x}}_i)^\top \boldsymbol{\beta} - \tilde{y}_i)^2. \quad (4)$$

Analogously, (2) can be equivalently written as $\boldsymbol{\theta}_S = \mathbf{U}_S \boldsymbol{\beta}_S$ where

$$\boldsymbol{\beta}_S = \underset{\boldsymbol{\beta} \in \mathbb{R}^{d_S}}{\operatorname{argmin}} \frac{1}{N} \sum_{i=1}^N (\phi_S(\mathbf{x}_i)^\top \boldsymbol{\beta} - f_T(\mathbf{x}_i))^2. \quad (5)$$

C.1 SFT of Weak Teacher

We start by considering the population-optimal linear predictor over the weak teacher representation, $\phi_T(\cdot)$: as $n \rightarrow \infty$, (4) converges to

$$\boldsymbol{\beta}_T^\infty = \underset{\boldsymbol{\beta} \in \mathbb{R}^{d_T}}{\operatorname{argmin}} \mathbb{E}_{(\mathbf{x}, y) \sim \mathcal{D}_{\mathbf{x}, y}(\eta_\ell)} [(\phi_T(\mathbf{x})^\top \boldsymbol{\beta} - y)^2]. \quad (6)$$

Lemma 1 (Population SFT of weak teacher). *When supervisedly fine-tuned over the population, the weak teacher from (6) satisfies $f_T^\infty(\mathbf{x}) = \phi_T(\mathbf{x})^\top \boldsymbol{\beta}_T^\infty = \mathbf{z}(\mathbf{x})^\top \boldsymbol{\beta}_* = f_*$.*

Proof of Lemma 1. Notice that (6) admits a closed-form solution

$$\boldsymbol{\beta}_T^\infty = \boldsymbol{\Sigma}_{\phi_T, \eta_\ell}^{-1} \boldsymbol{\mu}_{\phi_T, \eta_\ell}, \quad \boldsymbol{\Sigma}_{\phi_T, \eta_\ell} = \mathbb{E}_{\mathcal{D}(\eta_\ell)} [\phi_T(\mathbf{x}) \phi_T(\mathbf{x})^\top], \quad \boldsymbol{\mu}_{\phi_T, \eta_\ell} = \mathbb{E}_{\mathcal{D}(\eta_\ell)} [\phi_T(\mathbf{x}) y].$$

Since $\mathbf{z}(\mathbf{x})$ and $\mathbf{w}(\mathbf{x})$ are independent, we have

$$\begin{aligned} \boldsymbol{\Sigma}_{\phi_T, \eta_\ell} &= \mathbb{E}_{\mathcal{D}(\eta_\ell)} \left[(\mathbf{z}(\mathbf{x}) \otimes \mathbf{w}(\mathbf{x})) (\mathbf{z}(\mathbf{x}) \otimes \mathbf{w}(\mathbf{x}))^\top \right] \\ &= \mathbb{E}_{\mathcal{D}(\eta_\ell)} [\mathbf{z}(\mathbf{x}) \mathbf{z}(\mathbf{x})^\top] \otimes \mathbb{E}_{\mathcal{D}(\eta_\ell)} [\mathbf{w}(\mathbf{x}) \mathbf{w}(\mathbf{x})^\top] \\ &= \mathbf{I}_{d_z} \otimes \mathbf{C}_T(\eta_\ell), \end{aligned} \quad (7)$$

where

$$\mathbf{C}_T(\eta_\ell) = \begin{bmatrix} 1 & \eta_\ell \boldsymbol{\mu}_T^\top \\ \eta_\ell \boldsymbol{\mu}_T & \sigma_\xi^2 \mathbf{I}_{p_T-1} + \eta_\ell^2 \boldsymbol{\mu}_T \boldsymbol{\mu}_T^\top \end{bmatrix} = \operatorname{diag}(0, \sigma_\xi^2 \mathbf{I}_{p_T-1}) + \begin{bmatrix} 1 \\ \eta_\ell \boldsymbol{\mu}_T \end{bmatrix} \begin{bmatrix} 1 & \eta_\ell \boldsymbol{\mu}_T \end{bmatrix}, \quad (8)$$

whose inverse can be computed via block matrix inversion as

$$\mathbf{C}_T(\eta_\ell)^{-1} = \begin{bmatrix} 1 + \sigma_\xi^{-2} \|\eta_\ell \boldsymbol{\mu}_T\|_2^2 & -\sigma_\xi^{-2} \eta_\ell \boldsymbol{\mu}_T^\top \\ -\sigma_\xi^{-2} \eta_\ell \boldsymbol{\mu}_T & \sigma_\xi^{-2} \mathbf{I}_{p_T-1} \end{bmatrix}. \quad (9)$$

Meanwhile, by the independence of $\mathbf{z}(\mathbf{x})$ and $\mathbf{w}(\mathbf{x})$, we have

$$\begin{aligned} \boldsymbol{\mu}_{\phi_T, \eta_\ell} &= \mathbb{E}_{\mathcal{D}(\eta_\ell)} [\mathbf{z}(\mathbf{x}) \otimes \mathbf{w}(\mathbf{x}) (\mathbf{z}(\mathbf{x})^\top \boldsymbol{\beta}_* + \epsilon)] \\ &= (\mathbb{E}_{\mathcal{D}(\eta_\ell)} [\mathbf{z}(\mathbf{x}) \mathbf{z}(\mathbf{x})^\top] \boldsymbol{\beta}_*) \otimes \mathbb{E}_{\mathcal{D}(\eta_\ell)} [\mathbf{w}(\mathbf{x})] \\ &= \boldsymbol{\beta}_* \otimes \begin{bmatrix} 1 \\ \eta_\ell \boldsymbol{\mu}_T \end{bmatrix}. \end{aligned}$$

Therefore, the population-optimal linear predictor over ϕ_T is given by

$$\begin{aligned} \boldsymbol{\beta}_T^\infty &= \boldsymbol{\Sigma}_{\phi_T, \eta_\ell}^{-1} \boldsymbol{\mu}_{\phi_T, \eta_\ell} = (\mathbf{I}_{d_z} \otimes \mathbf{C}_T(\eta_\ell))^{-1} \left(\boldsymbol{\beta}_* \otimes \begin{bmatrix} 1 \\ \eta_\ell \boldsymbol{\mu}_T \end{bmatrix} \right) = \boldsymbol{\beta}_* \otimes \left(\mathbf{C}_T(\eta_\ell)^{-1} \begin{bmatrix} 1 \\ \eta_\ell \boldsymbol{\mu}_T \end{bmatrix} \right) \\ &= \boldsymbol{\beta}_* \otimes \left(\begin{bmatrix} 1 + \sigma_\xi^{-2} \|\eta_\ell \boldsymbol{\mu}_T\|_2^2 & -\sigma_\xi^{-2} \eta_\ell \boldsymbol{\mu}_T^\top \\ -\sigma_\xi^{-2} \eta_\ell \boldsymbol{\mu}_T & \sigma_\xi^{-2} \mathbf{I}_{p_T-1} \end{bmatrix} \begin{bmatrix} 1 \\ \eta_\ell \boldsymbol{\mu}_T \end{bmatrix} \right) = \boldsymbol{\beta}_* \otimes \mathbf{e}_1, \end{aligned}$$

where $\mathbf{e}_1 \in \mathbb{R}^{p_T}$ is the first canonical basis. \square

While the $f_T^\infty = f_*$ achieves the optimal population risk $\mathcal{R}(f_T^\infty) = \mathcal{R}(f_*) = \sigma_y^2$, the inefficient representation ($d_T = d_z p_T \gg d_z$) and the entangled features of ϕ_T make the finite-sample generalization challenging, especially under spurious correlations, as we will show next.

Theorem 1 (SFT of weak teacher (Section C.1)). *Under Assumptions 1 to 3, (1) satisfies*

$$\mathbb{E}_{\mathcal{D}(\eta_\ell)^n} [\mathbf{ER}_{\eta_t}(f_T)] \xrightarrow{\mathbb{P}} \sigma_y^2 \gamma_z \left(\underbrace{p_T}_{\mathcal{V}_T^{(0)} \text{ from variance}} + \underbrace{\frac{\|(\eta_t - \eta_\ell) \boldsymbol{\mu}_T\|_2^2}{\sigma_\xi^2}}_{\mathcal{V}_T^{(1)} \text{ from spurious correlations}} \right).$$

Proof of Theorem 1. For a small labeled set $\tilde{\mathcal{S}} = \{(\tilde{\mathbf{x}}_i, \tilde{y}_i) \mid i \in [n]\} \sim \mathcal{D}(\eta_\ell)^n$, the SFT in (1) admits a closed-form solution

$$\boldsymbol{\beta}_T = (\tilde{\boldsymbol{\Phi}}_T^\top \tilde{\boldsymbol{\Phi}}_T)^{-1} \tilde{\boldsymbol{\Phi}}_T^\top \tilde{\mathbf{y}}, \quad (10)$$

where $\tilde{\boldsymbol{\Phi}}_T = [\phi_T(\tilde{\mathbf{x}}_1), \dots, \phi_T(\tilde{\mathbf{x}}_n)]^\top \in \mathbb{R}^{n \times d_T}$ and $\tilde{\mathbf{y}} = [\tilde{y}_1, \dots, \tilde{y}_n]^\top \in \mathbb{R}^n$. Since Lemma 1 shows that the population-optimal linear predictor over ϕ_T is $f_T^\infty(\mathbf{x}) = \phi_T(\mathbf{x})^\top \boldsymbol{\beta}_T^\infty = f_*(\mathbf{x})$, we have $\tilde{\mathbf{y}} = \tilde{\boldsymbol{\Phi}}_T \boldsymbol{\beta}_T^\infty + \tilde{\boldsymbol{\epsilon}}$ where $\tilde{\boldsymbol{\epsilon}} \sim \mathcal{N}(\mathbf{0}_n, \sigma_y^2 \mathbf{I}_n)$. Therefore, we observe that

$$\boldsymbol{\beta}_T - \boldsymbol{\beta}_T^\infty = (\tilde{\boldsymbol{\Phi}}_T^\top \tilde{\boldsymbol{\Phi}}_T)^{-1} \tilde{\boldsymbol{\Phi}}_T^\top \tilde{\boldsymbol{\epsilon}}.$$

Since the excess risk over the test distribution $\mathcal{D}(\eta_t)$ is given by

$$\begin{aligned} \mathbf{ER}_{\eta_t}(f_T) &= \mathbb{E}_{\mathcal{D}(\eta_t)}[(f_T(\mathbf{x}) - f_*(\mathbf{x}))^2] = \mathbb{E}_{\mathcal{D}(\eta_t)}[(\phi_T(\mathbf{x})^\top (\boldsymbol{\beta}_T - \boldsymbol{\beta}_T^\infty))^2] \\ &= \|\boldsymbol{\beta}_T - \boldsymbol{\beta}_T^\infty\|_{\boldsymbol{\Sigma}_{\phi_T, \eta_t}}^2, \end{aligned}$$

where $\boldsymbol{\Sigma}_{\phi_T, \eta_t} = \mathbb{E}_{\mathcal{D}(\eta_t)}[\phi_T(\mathbf{x}) \phi_T(\mathbf{x})^\top]$, let $\tilde{\boldsymbol{\Sigma}}_n = \frac{1}{n} \tilde{\boldsymbol{\Phi}}_T^\top \tilde{\boldsymbol{\Phi}}_T \in \mathbb{R}^{d_T \times d_T}$ be the sample covariance matrix of $\phi_T(\tilde{\mathbf{x}})$ over $\tilde{\mathbf{x}} \sim \mathcal{D}_{\mathbf{x}}(\eta_\ell)$, we have

$$\begin{aligned} \mathbb{E}_{\tilde{\mathcal{S}} \sim \mathcal{D}(\eta_\ell)^n} [\mathbf{ER}_{\eta_t}(f_T)] &= \text{tr} \left(\mathbb{E}_{\tilde{\mathcal{S}} \sim \mathcal{D}(\eta_\ell)^n} \left[\boldsymbol{\Sigma}_{\phi_T, \eta_t} (\boldsymbol{\beta}_T - \boldsymbol{\beta}_T^\infty) (\boldsymbol{\beta}_T - \boldsymbol{\beta}_T^\infty)^\top \right] \right) \\ &= \sigma_y^2 \text{tr} \left(\boldsymbol{\Sigma}_{\phi_T, \eta_t} \mathbb{E}_{\tilde{\mathcal{S}} \sim \mathcal{D}(\eta_\ell)^n} \left[(\tilde{\boldsymbol{\Phi}}_T^\top \tilde{\boldsymbol{\Phi}}_T)^{-1} \right] \right) \\ &= \frac{\sigma_y^2}{n} \text{tr} \left(\boldsymbol{\Sigma}_{\phi_T, \eta_t} \tilde{\boldsymbol{\Sigma}}_n^{-1} \right). \end{aligned} \quad (11)$$

Recall $\phi_T(\mathbf{x}) = \mathbf{z}(\mathbf{x}) \otimes \mathbf{w}(\mathbf{x})$ and notice that for any $\eta \in [0, 1]$,

$$\mathbb{E}_{\mathcal{D}(\eta)}[\phi_T(\mathbf{x})] = \mathbb{E}_{\mathcal{D}(\eta)}[\mathbf{z}(\mathbf{x})] \otimes \mathbb{E}_{\mathcal{D}(\eta)}[\mathbf{w}(\mathbf{x})] = \mathbf{0}_{d_T},$$

while the derivation of (7) suggests that for any $\eta \in [0, 1]$,

$$\boldsymbol{\Sigma}_{\phi_T, \eta} = \mathbb{E}_{\mathcal{D}(\eta)}[\phi_T(\mathbf{x}) \phi_T(\mathbf{x})^\top] = \mathbf{I}_{d_z} \otimes \mathbf{C}_T(\eta). \quad (12)$$

However, we notice that $\phi_T(\mathbf{x})$ is not multivariate Gaussian due to the non-Gaussianity of products of independent Gaussian variables and the dependence of entries in $\mathbf{z}(\mathbf{x}) \otimes \mathbf{w}(\mathbf{x})$. Therefore, $\tilde{\boldsymbol{\Sigma}}_n$ cannot be directly computed using inverse Wishart. Instead, we leverage the concentration of $\tilde{\boldsymbol{\Sigma}}_n$ in the proportional asymptotic limit (Assumption 3). In particular, Lemma 2 and (12) implies that as $d_z, n \rightarrow \infty$ with $d_z/n \rightarrow \gamma_z \in (0, p_T^{-1})$,

$$\frac{\sigma_y^2}{n} \text{tr} \left(\boldsymbol{\Sigma}_{\phi_T, \eta_t} \tilde{\boldsymbol{\Sigma}}_n^{-1} \right) \xrightarrow{\mathbb{P}} \sigma_y^2 \gamma_z \text{tr} \left(\mathbf{C}_T(\eta_t) \mathbf{C}_T(\eta_t)^{-1} \right). \quad (13)$$

Leveraging the derivation of (8) and (9), we observe that

$$\begin{aligned}\text{tr}(\mathbf{C}_T(\eta_t)\mathbf{C}_T(\eta_\ell)^{-1}) &= p_T + \sigma_\xi^{-2}\eta_\ell^2\|\boldsymbol{\mu}_T\|_2^2 - 2\sigma_\xi^{-2}\eta_t\eta_\ell\|\boldsymbol{\mu}_T\|_2^2 + \sigma_\xi^{-2}\eta_t^2\|\boldsymbol{\mu}_T\|_2^2 \\ &= p_T + \sigma_\xi^{-2}(\eta_t - \eta_\ell)^2\|\boldsymbol{\mu}_T\|_2^2 = p_T + (\eta_t - \eta_\ell)^2\frac{\|\boldsymbol{\mu}_T\|_2^2}{\sigma_\xi^2},\end{aligned}\quad (14)$$

and therefore, (13) becomes

$$\begin{aligned}\frac{\sigma_y^2}{n} \text{tr}(\boldsymbol{\Sigma}_{\phi_T, \eta_t} \tilde{\boldsymbol{\Sigma}}_n^{-1}) &\xrightarrow{\mathbb{P}} \sigma_y^2 \frac{d_z}{n} \left(p_T + (\eta_t - \eta_\ell)^2 \frac{\|\boldsymbol{\mu}_T\|_2^2}{\sigma_\xi^2} \right) \\ &= \sigma_y^2 \gamma_z \left(p_T + (\eta_t - \eta_\ell)^2 \frac{\|\boldsymbol{\mu}_T\|_2^2}{\sigma_\xi^2} \right).\end{aligned}$$

Plugging the above into (11) completes the proof. \square

Lemma 2. For fixed $p_T \geq 2$, let $\mathbf{C} \in \mathbb{R}^{p_T \times p_T}$ be any fixed symmetric matrix with $\|\mathbf{C}\|_2 < \infty$. Recall $\tilde{\boldsymbol{\Sigma}}_n = \frac{1}{n} \sum_{i=1}^n \phi_T(\tilde{\mathbf{x}}_i) \phi_T(\tilde{\mathbf{x}}_i)^\top$ where $\tilde{\mathbf{x}}_i \sim \mathcal{D}_{\mathbf{x}}(\eta_\ell)$ i.i.d. for all $i \in [n]$. As $d_z, n \rightarrow \infty$ with $d_z/n \rightarrow \gamma_z \in (0, p_T^{-1})$,

$$\frac{1}{n} \text{tr}((\mathbf{I}_{d_z} \otimes \mathbf{C}) \tilde{\boldsymbol{\Sigma}}_n^{-1}) \xrightarrow{\mathbb{P}} \gamma_z \text{tr}(\mathbf{C} \mathbf{C}_T(\eta_\ell)^{-1}).$$

Proof of Lemma 2. We observe that $\phi_T(\mathbf{x})\phi_T(\mathbf{x})^\top = (\mathbf{z}(\mathbf{x})\mathbf{z}(\mathbf{x})^\top) \otimes (\mathbf{w}(\mathbf{x})\mathbf{w}(\mathbf{x})^\top)$, and the sample covariance matrix $\tilde{\boldsymbol{\Sigma}}_n$ can be partitioned into $d_z \times d_z$ blocks of size $p_T \times p_T$:

$$\tilde{\boldsymbol{\Sigma}}_n = \left[\tilde{\boldsymbol{\Sigma}}_n^{(k,l)} \right]_{k,l \in [d_z]} \quad \text{where} \quad \tilde{\boldsymbol{\Sigma}}_n^{(k,l)} = \frac{1}{n} \sum_{i=1}^n z_k(\tilde{\mathbf{x}}_i) z_l(\tilde{\mathbf{x}}_i) \cdot \mathbf{w}(\tilde{\mathbf{x}}_i) \mathbf{w}(\tilde{\mathbf{x}}_i)^\top \in \mathbb{R}^{p_T \times p_T},$$

where for any $\mathbf{x} \in \mathcal{X}$, $z_k(\mathbf{x})$ is the k -th entry of $\mathbf{z}(\mathbf{x})$. Notice that $\mathbb{E}[\tilde{\boldsymbol{\Sigma}}_n^{(k,l)}] = \delta_{k,l} \mathbf{C}_T(\eta_\ell)$ where $\delta_{k,l}$ is the Kronecker delta since $\mathbf{z}(\mathbf{x})$ and $\mathbf{w}(\mathbf{x})$ are independent, and $\mathbb{E}[z_k(\mathbf{x})z_l(\mathbf{x})] = \delta_{k,l}$ given $\mathbf{z}(\mathbf{x}) \sim \mathcal{N}(\mathbf{0}_{d_z}, \mathbf{I}_{d_z})$.

Off-diagonal blocks are negligible. For any $k, l \in [d_z]$ with $k \neq l$, we define $p_T \times p_T$ self-adjoint matrices,

$$\mathbf{Y}_i^{(k,l)} := \frac{1}{n} z_k(\tilde{\mathbf{x}}_i) z_l(\tilde{\mathbf{x}}_i) (\mathbf{w}(\tilde{\mathbf{x}}_i) \mathbf{w}(\tilde{\mathbf{x}}_i)^\top - \mathbf{C}_T(\eta_\ell)) \quad \text{and} \quad \mathbf{R}_i^{(k,l)} := \frac{1}{n} z_k(\tilde{\mathbf{x}}_i) z_l(\tilde{\mathbf{x}}_i) \mathbf{C}_T(\eta_\ell),$$

where recall from the derivation of (7) that $\mathbf{C}_T(\eta_\ell) = \mathbb{E}_{\mathcal{D}(\eta_\ell)}[\mathbf{w}(\mathbf{x}) \mathbf{w}(\mathbf{x})^\top]$. Since $\mathbb{E}[z_k(\mathbf{x})z_l(\mathbf{x})] = \delta_{k,l}$, we have $\mathbb{E}[\mathbf{Y}_i^{(k,l)}] = \mathbb{E}[\mathbf{R}_i^{(k,l)}] = \mathbf{0}_{p_T \times p_T}$ for $k \neq l$, and

$$\tilde{\boldsymbol{\Sigma}}_n^{(k,l)} = \sum_{i=1}^n \mathbf{Y}_i^{(k,l)} + \mathbf{R}_i^{(k,l)}, \quad \mathbb{E}[\tilde{\boldsymbol{\Sigma}}_n^{(k,l)}] = \mathbf{0}_{p_T \times p_T}.$$

Let $L_n := 4\sqrt{\log(n)}$ and consider the event

$$E_n := \left\{ \max_{i \in [n]} \|\mathbf{z}(\tilde{\mathbf{x}}_i)\|_\infty^2 \leq L_n^2 \right\} \wedge \left\{ \max_{i \in [n]} \|\mathbf{w}(\tilde{\mathbf{x}}_i)\|_2^2 \leq L_n^2 \right\}.$$

First, for $\mathbf{z}(\tilde{\mathbf{x}}_i) \sim \mathcal{N}(\mathbf{0}_{d_z}, \mathbf{I}_{d_z})$, the union bound and Gaussian tail bound imply that

$$\begin{aligned} \Pr \left[\max_{i \in [n]} \|\mathbf{z}(\tilde{\mathbf{x}}_i)\|_\infty > \frac{L_n}{\sqrt{2}} \right] &= \Pr \left[\max_{i \in [n], k \in [d_z]} |z_k(\tilde{\mathbf{x}}_i)| > \frac{L_n}{\sqrt{2}} \right] \\ &\leq 2nd_z \exp \left(-\frac{L_n^2}{4} \right) = \frac{2d_z}{n} \cdot n^{-2} = o(n^{-1}). \end{aligned}$$

Meanwhile, we observe that for $\mathbf{g}_i \sim \mathcal{N}(\mathbf{0}_{p_T-1}, \mathbf{I}_{p_T-1})$,

$$\|\mathbf{w}(\tilde{\mathbf{x}}_i)\|_2^2 = 1 + \left\| [\mathbf{w}(\tilde{\mathbf{x}}_i)]_{2:p_T} \right\|_2^2 \leq 2\eta_\ell^2 \|\boldsymbol{\mu}_T\|_2^2 + 2\sigma_\xi^2 \|\mathbf{g}_i\|_2^2,$$

while the Laurent-Massart χ^2 tail bound [Laurent and Massart, 2000] implies that

$$\Pr \left[\|\mathbf{g}_i\|_2^2 > p_T - 1 + 2\sqrt{(p_T - 1)t} + 2t \right] \leq e^{-t}, \quad \forall t > 0.$$

Then, for fixed and finite p_T and $\|\boldsymbol{\mu}_T\|_2$, with a sufficiently large n , there exists a constant $a_n > 1/8$ such that applying the union bound with $t = a_n L_n^2$ yields that

$$\Pr \left[\max_{i \in [n]} \|\mathbf{w}(\tilde{\mathbf{x}}_i)\|_2^2 > L_n^2 \right] \leq n \exp(-a_n L_n^2) = o(n^{-1}).$$

Applying the union bound again, we get $\Pr[E_n^c] = o(n^{-1})$ for sufficiently large n . Meanwhile, conditioned on E_n , we have for any $i \in [n]$,

$$\left\| \mathbf{Y}_i^{(k,l)} \right\|_2 \leq \frac{1}{n} \|\mathbf{z}(\tilde{\mathbf{x}}_i)\|_\infty^2 \|\mathbf{w}(\tilde{\mathbf{x}}_i)\|_2^2 \leq \frac{L_n^4}{n}, \quad \left\| \mathbf{R}_i^{(k,l)} \right\|_2 \leq \frac{1}{n} \|\mathbf{z}(\tilde{\mathbf{x}}_i)\|_\infty^2 \|\mathbf{C}_T(\eta_\ell)\|_2 \lesssim \frac{L_n^2}{n},$$

which implies that

$$\begin{aligned} \left\| \sum_{i=1}^n \mathbb{E} \left[(\mathbf{Y}_i^{(k,l)})^2 \mid E_n \right] \right\|_2 &\leq \sum_{i=1}^n \mathbb{E} \left[\left\| \mathbf{Y}_i^{(k,l)} \right\|_2^2 \mid E_n \right] \leq n \cdot \frac{L_n^8}{n^2} = \frac{L_n^8}{n}, \\ \left\| \sum_{i=1}^n \mathbb{E} \left[(\mathbf{R}_i^{(k,l)})^2 \mid E_n \right] \right\|_2 &\leq \sum_{i=1}^n \mathbb{E} \left[\left\| \mathbf{R}_i^{(k,l)} \right\|_2^2 \mid E_n \right] \lesssim n \cdot \frac{L_n^4}{n^2} = \frac{L_n^4}{n}. \end{aligned}$$

Then, applying the matrix Bernstein inequality [Tropp, 2012, Theorem 1.6] to $\sum_{i=1}^n \mathbf{Y}_i^{(k,l)}$ and $\sum_{i=1}^n \mathbf{R}_i^{(k,l)}$ and a union bound over all $k, l \in [d_z]$ off-diagonal blocks with $k \neq l$ yields that

$$\begin{aligned} \Pr \left[\max_{k \neq l} \left\| \tilde{\boldsymbol{\Sigma}}_n^{(k,l)} \right\|_2 \gtrsim \sqrt{\frac{\log(n)}{n}} \right] &\leq \Pr [E_n^c] + \Pr \left[\max_{k \neq l} \left\| \tilde{\boldsymbol{\Sigma}}_n^{(k,l)} \right\|_2 \gtrsim \sqrt{\frac{\log(n)}{n}} \mid E_n \right] \\ &\leq o(n^{-1}) + 2p_T n^{-\Omega\left(\frac{n^2}{\log^4(n)}\right)} \cdot d_z^2 = o(1), \end{aligned}$$

and therefore, the off-diagonal blocks are negligible:

$$\max_{k \neq l} \left\| \tilde{\boldsymbol{\Sigma}}_n^{(k,l)} \right\|_2 = O_{\mathbb{P}} \left(\sqrt{\frac{\log(n)}{n}} \right).$$

Diagonal blocks are concentrated. Consider the k -th diagonal block $\tilde{\Sigma}_n^{(k,k)}$ for any fixed $k \in [d_z]$:

$$\begin{aligned}\tilde{\Sigma}_n^{(k,k)} &= \frac{1}{n} \sum_{i=1}^n z_k(\tilde{\mathbf{x}}_i)^2 \cdot \mathbf{w}(\tilde{\mathbf{x}}_i) \mathbf{w}(\tilde{\mathbf{x}}_i)^\top \\ &= \frac{1}{n} \sum_{i=1}^n \mathbf{w}(\tilde{\mathbf{x}}_i) \mathbf{w}(\tilde{\mathbf{x}}_i)^\top + \frac{1}{n} \sum_{i=1}^n (z_k(\tilde{\mathbf{x}}_i)^2 - 1) \cdot \mathbf{w}(\tilde{\mathbf{x}}_i) \mathbf{w}(\tilde{\mathbf{x}}_i)^\top,\end{aligned}$$

where we denote $\hat{\mathbf{C}}_{T,n} = \frac{1}{n} \sum_{i=1}^n \mathbf{w}(\tilde{\mathbf{x}}_i) \mathbf{w}(\tilde{\mathbf{x}}_i)^\top$. Let

$$s_k := \frac{1}{n} \sum_{i=1}^n z_k(\tilde{\mathbf{x}}_i)^2. \quad (15)$$

Then,

$$\tilde{\Sigma}_n^{(k,k)} - s_k \mathbf{C}_T(\eta_\ell) = (\hat{\mathbf{C}}_{T,n} - \mathbf{C}_T(\eta_\ell)) + \frac{1}{n} \sum_{i=1}^n (z_k(\tilde{\mathbf{x}}_i)^2 - 1) \cdot (\mathbf{w}(\tilde{\mathbf{x}}_i) \mathbf{w}(\tilde{\mathbf{x}}_i)^\top - \mathbf{C}_T(\eta_\ell)),$$

where both terms are sums of independent random matrices with zero mean. Leveraging the same argument as for the off-diagonal blocks using the same event E_n , the matrix Bernstein inequality [Tropp, 2012, Theorem 1.6], and a union bound over all $k \in [d_z]$, we have for sufficiently large n ,

$$\max_{k \in [d_z]} \left\| \tilde{\Sigma}_n^{(k,k)} - s_k \mathbf{C}_T(\eta_\ell) \right\|_2 = O_{\mathbb{P}} \left(\sqrt{\frac{\log(n)}{n}} \right). \quad (16)$$

Also, the χ^2 concentration [Laurent and Massart, 2000] implies that for any fixed $\epsilon \in (0, 1/2)$, as $d_z, n \rightarrow \infty$ with $d_z/n \rightarrow \gamma_z \in (0, p_T^{-1})$,

$$\begin{aligned}\Pr \left[\min_{k \in [d_z]} s_k < 1 - \epsilon \right] &\leq d_z \Pr [s_k < 1 - \epsilon] \leq d_z \exp(-\Theta(n\epsilon^2)) = o(1), \\ \Pr \left[\max_{k \in [d_z]} s_k > 1 + \epsilon \right] &\leq d_z \Pr [s_k > 1 + \epsilon] \leq d_z \exp(-\Theta(n\epsilon^2)) = o(1),\end{aligned} \quad (17)$$

so that all s_k 's are close to 1 with high probability.

Concentration of $\tilde{\Sigma}_n^{-1}$. Let $\mathbf{D}_n = \text{diag}(s_1 \mathbf{C}_T(\eta_\ell), \dots, s_{d_z} \mathbf{C}_T(\eta_\ell))$ be the block-diagonal matrix with k -th diagonal block $s_k \mathbf{C}_T(\eta_\ell)$ for all $k \in [d_z]$; and $\mathbf{E}_n = \tilde{\Sigma}_n - \mathbf{D}_n$ be the fluctuations around \mathbf{D}_n . Since $\mathbf{C}_T(\eta_\ell)$ is positive definite, (17) implies that $\|\mathbf{D}_n^{-1}\|_2 < \infty$ with high probability for sufficiently large n . Then, the resolvent identity implies that

$$\tilde{\Sigma}_n^{-1} = (\mathbf{D}_n + \mathbf{E}_n)^{-1} = \mathbf{D}_n^{-1} - \mathbf{D}_n^{-1} \mathbf{E}_n (\mathbf{D}_n + \mathbf{E}_n)^{-1}. \quad (18)$$

In particular, the block matrix inversion formula implies that for any $k \in [d_z]$, the k -th diagonal block of $\tilde{\Sigma}_n^{-1}$, denoted as $(\tilde{\Sigma}_n^{-1})^{(k,k)} \in \mathbb{R}^{p_T \times p_T}$ is concentrated around the k -th diagonal block of \mathbf{D}_n^{-1} , $(s_k \mathbf{C}_T(\eta_\ell))^{-1}$:

$$\left\| (\tilde{\Sigma}_n^{-1})^{(k,k)} - (s_k \mathbf{C}_T(\eta_\ell))^{-1} \right\|_2 \lesssim \|\mathbf{E}_n\|_2 = O_{\mathbb{P}} \left(\sqrt{\frac{\log(n)}{n}} \right), \quad (19)$$

Concentration of the trace. Finally, notice that the trace of interest, $\frac{1}{n} \text{tr} \left((\mathbf{I}_{d_z} \otimes \mathbf{C}) \tilde{\Sigma}_n^{-1} \right)$, depends only on the diagonal blocks of $\tilde{\Sigma}_n^{-1}$. Then, (19) implies that

$$\begin{aligned} \frac{1}{n} \text{tr} \left((\mathbf{I}_{d_z} \otimes \mathbf{C}) \tilde{\Sigma}_n^{-1} \right) &= \frac{1}{n} \sum_{k=1}^{d_z} \text{tr} \left(\mathbf{C} (\tilde{\Sigma}_n^{-1})^{(k,k)} \right) \\ &= \left(\frac{1}{n} \sum_{k=1}^{d_z} \frac{1}{s_k} \right) \text{tr} \left(\mathbf{C} \mathbf{C}_T (\eta_\ell)^{-1} \right) + O_{\mathbb{P}} \left(\sqrt{\frac{\log(n)}{n}} \right) \\ &= \left(\frac{1}{d_z} \sum_{k=1}^{d_z} \frac{1}{s_k} \right) \cdot \frac{d_z}{n} \text{tr} \left(\mathbf{C} \mathbf{C}_T (\eta_\ell)^{-1} \right) + o_{\mathbb{P}}(1). \end{aligned}$$

Since $\{ns_k\}_{k=1}^{d_z}$ are independent and χ_n^2 distributed, for any fixed $n > 2$, $\mathbb{E}[s_k^{-1}] = \frac{n}{n-2}$. Then, the weak law of large numbers implies that as $d_z, n \rightarrow \infty$,

$$\frac{1}{d_z} \sum_{k=1}^{d_z} \frac{1}{s_k} \xrightarrow{\mathbb{P}} \frac{n}{n-2} \xrightarrow{n \rightarrow \infty} 1.$$

Putting everything together with $d_z/n \rightarrow \gamma_z \in (0, p_T^{-1})$ completes the proof. \square

C.2 W2S Fine-tuning of Strong Student

Theorem 3 (W2S fine-tuning of strong student (formal restatement of Theorem 2)). *Under Assumptions 1 to 3, as $d_z, n, N \rightarrow \infty$ with $d_z/n \rightarrow \gamma_z \in (0, p_T^{-1})$ and $d_z/N \rightarrow \nu_z \in (0, p_S^{-1})$, $f_S(\mathbf{x}) = \varphi_S(\mathbf{x})^\top \boldsymbol{\theta}_S = \phi_S(\mathbf{x})^\top \boldsymbol{\beta}_S$ from (2) satisfies*

$$\begin{aligned} \mathbb{E}_{\mathcal{S}_x \sim \mathcal{D}(\eta_u)^N, \tilde{\mathcal{S}} \sim \mathcal{D}(\eta_\ell)^n} [\mathbf{ER}_{\eta_t}(f_S)] &\xrightarrow{\mathbb{P}} \sigma_y^2 \gamma_z \left(\frac{p_{T \wedge S}}{p_{T \wedge S}} + \right. \\ &\quad \left. \color{red} \mathcal{V}_S^{(0)} \leq \mathcal{V}_T^{(0)} \right) \\ &\quad \boxed{\frac{\|(\eta_u - \eta_\ell) \boldsymbol{\mu}_T + (\eta_t - \eta_u) \boldsymbol{\Xi} \boldsymbol{\mu}_S\|_2^2}{\sigma_\xi^2}} + \\ &\quad \color{blue} \mathcal{V}_S^{(1)} \leq \mathcal{V}_T^{(1)} \text{ when } \eta_u = \eta_\ell \\ &\quad \boxed{\nu_z (p_T - p_{T \wedge S}) \left(p_S + (\eta_t - \eta_u)^2 \frac{\|\boldsymbol{\mu}_S\|_2^2}{\sigma_\xi^2} \right)}, \\ &\quad \color{orange} \mathcal{E}_S = \Theta(\nu_z) \ll 1 \text{ negligible when } \nu_z \ll 1 \end{aligned}$$

where $p_{T \wedge S} = 1 + \|\boldsymbol{\Xi}\|_F^2 \in [1, p_S]$ quantifies the effective dimension of group features learned by the strong student from the weak teacher.

Notice that in Theorem 3, $\mathcal{V}_S^{(0)} + \mathcal{V}_S^{(1)}$ is dominant and will be small if \mathbf{T}, \mathbf{S} are nearly orthogonal (i.e., $\|\boldsymbol{\Xi}\|_2 \approx 0$) and $\eta_u \approx \eta_t$; whereas \mathcal{E}_S tends to be much smaller than $\mathcal{V}_S^{(0)} + \mathcal{V}_S^{(1)}$, especially since unlabeled data is usually abundant compared to labeled data (i.e., $\nu_z \ll \gamma_z$).

Proof of Theorems 2 and 3. We first introduce some helpful notions for the proof. Recall $\phi_S(\mathbf{x}) = \mathbf{z}(\mathbf{x}) \otimes \boldsymbol{\psi}(\mathbf{x})$. Let $\boldsymbol{\Sigma}_{\phi_S, \eta} = \mathbb{E}_{\mathcal{D}(\eta)} [\phi_S(\mathbf{x}) \phi_S(\mathbf{x})^\top]$ for any $\eta \in [0, 1]$ and observe that

$$\boldsymbol{\Sigma}_{\phi_S, \eta} = \mathbf{I}_{d_z} \otimes \mathbf{C}_S(\eta), \quad \mathbf{C}_S(\eta) = \mathbb{E}_{\mathcal{D}(\eta)} [\boldsymbol{\psi}(\mathbf{x}) \boldsymbol{\psi}(\mathbf{x})^\top] = \begin{bmatrix} 1 & \eta \boldsymbol{\mu}_S^\top \\ \eta \boldsymbol{\mu}_S & \sigma_\xi^2 \mathbf{I}_{p_S-1} + \eta^2 \boldsymbol{\mu}_S \boldsymbol{\mu}_S^\top \end{bmatrix}. \quad (20)$$

The block matrix inversion formula implies that

$$\mathbf{C}_S(\eta)^{-1} = \begin{bmatrix} 1 + \sigma_\xi^{-2}\eta^2\|\boldsymbol{\mu}_S\|_2^2 & -\sigma_\xi^{-2}\eta\boldsymbol{\mu}_S^\top \\ -\sigma_\xi^{-2}\eta\boldsymbol{\mu}_S & \sigma_\xi^{-2}\mathbf{I}_{p_S-1} \end{bmatrix}. \quad (21)$$

Meanwhile, the cross covariance of the student-teacher representations under $\mathcal{D}(\eta)$ is given by

$$\begin{aligned} \boldsymbol{\Sigma}_{\phi_S, \phi_T, \eta} &= \mathbb{E}_{\mathcal{D}(\eta)}[\phi_S(\mathbf{x})\phi_T(\mathbf{x})^\top] = \mathbb{E}_{\mathcal{D}(\eta)}[(\mathbf{z}(\mathbf{x}) \otimes \boldsymbol{\psi}(\mathbf{x}))(\mathbf{z}(\mathbf{x}) \otimes \mathbf{w}(\mathbf{x}))^\top] \\ &= \mathbb{E}_{\mathcal{D}(\eta)}[\mathbf{z}(\mathbf{x})\mathbf{z}(\mathbf{x})^\top] \otimes \mathbb{E}_{\mathcal{D}(\eta)}[\boldsymbol{\psi}(\mathbf{x})\mathbf{w}(\mathbf{x})^\top] = \mathbf{I}_{d_z} \otimes \mathbf{A}(\eta), \end{aligned}$$

where

$$\mathbf{A}(\eta) = \mathbb{E}_{\mathcal{D}(\eta)}[\boldsymbol{\psi}(\mathbf{x})\mathbf{w}(\mathbf{x})^\top] = \mathbb{E}_{\mathcal{D}(\eta)}\left[\left[\begin{matrix} 1 \\ \mathbf{S}^\top \boldsymbol{\xi}(\mathbf{x}) \end{matrix}\right] \left[\begin{matrix} 1 & \boldsymbol{\xi}(\mathbf{x})^\top \mathbf{T} \end{matrix}\right]\right] \quad (22)$$

$$= \begin{bmatrix} 1 & \eta\boldsymbol{\mu}_T^\top \\ \eta\boldsymbol{\mu}_S & \sigma_\xi^2 \mathbf{S}^\top \mathbf{T} + \eta^2 \boldsymbol{\mu}_S \boldsymbol{\mu}_T^\top \end{bmatrix} \in \mathbb{R}^{p_S \times p_T}. \quad (23)$$

Close-form solution and population-optimal predictor of W2S fine-tuning. Given the equivalence between (2) and (5), we consider the latter throughout the proof. Adapting the notion from the proof of Theorem 1, given the labeled set $\tilde{\mathcal{S}} = \{(\tilde{\mathbf{x}}_i, \tilde{y}_i) \mid i \in [n]\} \sim \mathcal{D}(\eta_\ell)^n$ and the unlabeled set $\mathcal{S} = \{(\mathbf{x}_i, y_i) \mid i \in [N]\} \sim \mathcal{D}_x(\eta_u)^N$ with unknown y_i 's, we denote

$$\begin{aligned} \tilde{\boldsymbol{\Phi}}_T &= [\phi_T(\tilde{\mathbf{x}}_1), \dots, \phi_T(\tilde{\mathbf{x}}_n)]^\top \in \mathbb{R}^{n \times d_T}, \quad \tilde{\mathbf{y}} = [\tilde{y}_1, \dots, \tilde{y}_n]^\top \in \mathbb{R}^n, \\ \boldsymbol{\Phi}_S &= [\phi_S(\mathbf{x}_1), \dots, \phi_S(\mathbf{x}_N)]^\top \in \mathbb{R}^{N \times d_S}, \quad \boldsymbol{\Phi}_T = [\phi_T(\mathbf{x}_1), \dots, \phi_T(\mathbf{x}_N)]^\top \in \mathbb{R}^{N \times d_T}. \end{aligned}$$

Then, since $n > d_T$ and $N > d_S$ by Assumption 3, (5) admits a unique closed-form solution

$$\boldsymbol{\beta}_S = (\boldsymbol{\Phi}_S^\top \boldsymbol{\Phi}_S)^{-1} \boldsymbol{\Phi}_S^\top \boldsymbol{\Phi}_T \boldsymbol{\beta}_T \quad \text{where} \quad \boldsymbol{\beta}_T = (\tilde{\boldsymbol{\Phi}}_T^\top \tilde{\boldsymbol{\Phi}}_T)^{-1} \tilde{\boldsymbol{\Phi}}_T^\top \tilde{\mathbf{y}}$$

from (10). Recall from Lemma 1 that the population-optimal linear predictor over ϕ_T in Lemma 1 is $f_T^\infty(\mathbf{x}) = \phi_T(\mathbf{x})^\top \boldsymbol{\beta}_T^\infty = f_*(\mathbf{x})$ with $\boldsymbol{\beta}_T^\infty = \boldsymbol{\beta}_* \otimes \mathbf{e}_1$. Conditioned on $f_T^\infty(\mathbf{x})$, the population-optimal linear predictor over ϕ_S is given by

$$\begin{aligned} \boldsymbol{\beta}_S^\infty &= \mathbb{E}_{\mathcal{D}(\eta_u)}[\phi_S(\mathbf{x})\phi_S(\mathbf{x})^\top]^{-1} \mathbb{E}_{\mathcal{D}(\eta_u)}[\phi_S(\mathbf{x})\phi_T(\mathbf{x})^\top] \boldsymbol{\beta}_T^\infty \\ &= (\mathbf{I}_{d_z} \otimes \mathbf{C}_S(\eta_u))^{-1} (\mathbf{I}_{d_z} \otimes \mathbf{A}(\eta_u)) \boldsymbol{\beta}_T^\infty \\ &= (\mathbf{I}_{d_z} \otimes (\mathbf{C}_S(\eta_u)^{-1} \mathbf{A}(\eta_u))) (\boldsymbol{\beta}_* \otimes \mathbf{e}_1) \\ &= \boldsymbol{\beta}_* \otimes (\mathbf{C}_S(\eta_u)^{-1} \mathbf{A}(\eta_u) \mathbf{e}_1) = \boldsymbol{\beta}_* \otimes \mathbf{e}_1, \end{aligned}$$

which implies that $f_S^\infty(\mathbf{x}) = \phi_S(\mathbf{x})^\top \boldsymbol{\beta}_S^\infty = f_*(\mathbf{x})$, *i.e.*, a strong student W2S fine-tuned with pseudolabels from the Bayes-optimal weak teacher over the population is also Bayes-optimal. Therefore, the student estimator in (5) differs from $\boldsymbol{\beta}_S^\infty$ by

$$\begin{aligned} \boldsymbol{\beta}_S - \boldsymbol{\beta}_S^\infty &= (\boldsymbol{\Phi}_S^\top \boldsymbol{\Phi}_S)^{-1} \boldsymbol{\Phi}_S^\top \boldsymbol{\Phi}_T (\boldsymbol{\beta}_T - \boldsymbol{\beta}_T^\infty) \\ &= (\boldsymbol{\Phi}_S^\top \boldsymbol{\Phi}_S)^{-1} \boldsymbol{\Phi}_S^\top \boldsymbol{\Phi}_T (\tilde{\boldsymbol{\Phi}}_T^\top \tilde{\boldsymbol{\Phi}}_T)^{-1} \tilde{\boldsymbol{\Phi}}_T^\top \tilde{\boldsymbol{\epsilon}}, \end{aligned}$$

and the estimation error of W2S fine-tuning is given by

$$\mathbf{ER}_{\eta_t}(f_S) = \mathbb{E}_{\mathcal{D}(\eta_t)}[(f_S(\mathbf{x}) - f_*(\mathbf{x}))^2] = \mathbb{E}_{\mathcal{D}(\eta_t)}[(\phi_S(\mathbf{x})^\top (\boldsymbol{\beta}_S - \boldsymbol{\beta}_S^\infty))^2] = \|\boldsymbol{\beta}_S - \boldsymbol{\beta}_S^\infty\|_{\Sigma_{\phi_S, \eta_t}}^2.$$

Then, conditioned on $\tilde{\Phi}_T$ and Φ_S, Φ_T , the excess risk can be expressed as

$$\begin{aligned} & \mathbb{E}_{\tilde{\epsilon}} \left[\text{ER}_{\eta_t}(f_S) \mid \tilde{\Phi}_T, \Phi_S, \Phi_T \right] \\ &= \mathbb{E}_{\tilde{\epsilon}} \left[\left\| (\Phi_S^\top \Phi_S)^{-1} \Phi_S^\top \Phi_T (\tilde{\Phi}_T^\top \tilde{\Phi}_T)^{-1} \tilde{\Phi}_T^\top \tilde{\epsilon} \right\|_{\Sigma_{\phi_S, \eta_t}}^2 \mid \tilde{\Phi}_T, \Phi_S, \Phi_T \right] \\ &= \sigma_y^2 \text{tr} \left(\Sigma_{\phi_S, \eta_t} (\Phi_S^\top \Phi_S)^{-1} \Phi_S^\top \Phi_T (\tilde{\Phi}_T^\top \tilde{\Phi}_T)^{-1} \Phi_T^\top \Phi_S (\Phi_S^\top \Phi_S)^{-1} \right). \end{aligned} \quad (24)$$

Concentration of sample covariance matrices. Define the sample (cross) covariance matrices

$$\hat{\Sigma}_{S,N} = \frac{1}{N} \Phi_S^\top \Phi_S, \quad \hat{\Sigma}_{S,T,N} = \frac{1}{N} \Phi_S^\top \Phi_T, \quad \tilde{\Sigma}_{T,n} = \frac{1}{n} \tilde{\Phi}_T^\top \tilde{\Phi}_T.$$

Then, taking the expectation of (24) over $\tilde{\mathcal{S}}$ and \mathcal{S}_x yields

$$\mathbb{E}_{\tilde{\mathcal{S}}, \mathcal{S}_x} [\text{ER}_{\eta_t}(f_S)] = \frac{\sigma_y^2}{n} \text{tr} \left(\mathbb{E}_{\mathcal{S}_x} \left[\hat{\Sigma}_{S,T,N}^\top \hat{\Sigma}_{S,N}^{-1} \Sigma_{\phi_S, \eta_t} \hat{\Sigma}_{S,N}^{-1} \hat{\Sigma}_{S,T,N} \right] \mathbb{E}_{\tilde{\mathcal{S}}} \left[\tilde{\Sigma}_{T,n}^{-1} \right] \right). \quad (25)$$

At the proportional asymptotic limit, Lemma 3 below shows that

$$\begin{aligned} & \frac{1}{n} \text{tr} \left(\mathbb{E}_{\mathcal{S}_x} \left[\hat{\Sigma}_{S,T,N}^\top \hat{\Sigma}_{S,N}^{-1} \Sigma_{\phi_S, \eta_t} \hat{\Sigma}_{S,N}^{-1} \hat{\Sigma}_{S,T,N} \right] \mathbb{E}_{\tilde{\mathcal{S}}} \left[\tilde{\Sigma}_{T,n}^{-1} \right] \right) \\ & \xrightarrow{\mathbb{P}} \gamma_z \text{tr} (\mathbf{C}_{T,S}(\eta_t, \eta_u) \mathbf{C}_T(\eta_\ell)^{-1}) + \gamma_z \nu_z (p_T - p_{T \wedge S}) \text{tr} (\mathbf{C}_S(\eta_t) \mathbf{C}_S(\eta_u)^{-1}), \end{aligned}$$

Leveraging (20), (21), and (22), we have

$$\begin{aligned} \text{tr} (\mathbf{C}_{T,S}(\eta_t, \eta_u) \mathbf{C}_T(\eta_\ell)^{-1}) &= \text{tr} (\mathbf{A}(\eta_u)^\top \mathbf{C}_S(\eta_u)^{-1} \mathbf{C}_S(\eta_t) \mathbf{C}_S(\eta_u)^{-1} \mathbf{A}(\eta_u) \mathbf{C}_T(\eta_\ell)^{-1}) \\ &= 1 + \|\boldsymbol{\Xi}\|_F^2 + \frac{\|(\eta_u - \eta_\ell) \boldsymbol{\mu}_T + (\eta_t - \eta_u) \boldsymbol{\Xi} \boldsymbol{\mu}_S\|_2^2}{\sigma_\xi^2} \\ &= p_{T \wedge S} + \frac{\|(\eta_u - \eta_\ell) \boldsymbol{\mu}_T + (\eta_t - \eta_u) \boldsymbol{\Xi} \boldsymbol{\mu}_S\|_2^2}{\sigma_\xi^2}, \end{aligned}$$

while an analogous derivation as in (14) implies that

$$\text{tr} (\mathbf{C}_S(\eta_t) \mathbf{C}_S(\eta_u)^{-1}) = p_S + (\eta_t - \eta_u)^2 \frac{\|\boldsymbol{\mu}_S\|_2^2}{\sigma_\xi^2}.$$

Overall, plugging everything back to (25) yields

$$\begin{aligned} \mathbb{E}_{\tilde{\mathcal{S}}, \mathcal{S}_x} [\text{ER}_{\eta_t}(f_S)] &\xrightarrow{\mathbb{P}} \sigma_y^2 \gamma_z \left(p_{T \wedge S} + \frac{\|(\eta_u - \eta_\ell) \boldsymbol{\mu}_T + (\eta_t - \eta_u) \boldsymbol{\Xi} \boldsymbol{\mu}_S\|_2^2}{\sigma_\xi^2} \right) \\ &\quad + \sigma_y^2 \gamma_z \nu_z (p_T - p_{T \wedge S}) \left(p_S + (\eta_t - \eta_u)^2 \frac{\|\boldsymbol{\mu}_S\|_2^2}{\sigma_\xi^2} \right), \end{aligned}$$

□

Lemma 3. *In the proof of Theorem 2, at the proportional asymptotic limit,*

$$\begin{aligned} & \frac{1}{n} \text{tr} \left(\mathbb{E}_{\mathcal{S}_x} \left[\hat{\Sigma}_{S,T,N}^\top \hat{\Sigma}_{S,N}^{-1} \Sigma_{\phi_S, \eta_t} \hat{\Sigma}_{S,N}^{-1} \hat{\Sigma}_{S,T,N} \right] \mathbb{E}_{\tilde{\mathcal{S}}} \left[\tilde{\Sigma}_{T,n}^{-1} \right] \right) \\ & \xrightarrow{\mathbb{P}} \gamma_z \text{tr} (\mathbf{C}_{T,S}(\eta_t, \eta_u) \mathbf{C}_T(\eta_\ell)^{-1}) + \gamma_z \nu_z (p_T - p_{T \wedge S}) \text{tr} (\mathbf{C}_S(\eta_t) \mathbf{C}_S(\eta_u)^{-1}), \end{aligned}$$

where $\mathbf{C}_{T,S}(\eta_t, \eta_u) \in \mathbb{R}^{p_T \times p_T}$ is defined as

$$\mathbf{C}_{T,S}(\eta_t, \eta_u) = \mathbf{A}(\eta_u)^\top \mathbf{C}_S(\eta_u)^{-1} \mathbf{C}_S(\eta_t) \mathbf{C}_S(\eta_u)^{-1} \mathbf{A}(\eta_u),$$

Proof of Lemma 3. The proof mostly follows the same argument as in Lemma 2, with the key difference being a careful treatment of the off-diagonal blocks in the sample (cross) covariance matrices $\widehat{\Sigma}_{S,N}$ and $\widehat{\Sigma}_{S,T,N}$, which are still small but with an additional non-negligible higher-order moment in the proportional asymptotic limit.

Following the proof of Lemma 2, “Separation of block diagonals and off-diagonals”, we first partition $\widehat{\Sigma}_{S,N}$ and $\widehat{\Sigma}_{S,T,N}$ into $d_z \times d_z$ blocks:

$$\widehat{\Sigma}_{S,N} = \left[\widehat{\Sigma}_{S,N}^{(k,l)} \right]_{k,l=1}^{d_z}, \quad \widehat{\Sigma}_{S,T,N} = \left[\widehat{\Sigma}_{S,T,N}^{(k,l)} \right]_{k,l=1}^{d_z},$$

where $\widehat{\Sigma}_{S,N}^{(k,l)} \in \mathbb{R}^{p_S \times p_S}$ and $\widehat{\Sigma}_{S,T,N}^{(k,l)} \in \mathbb{R}^{p_S \times p_T}$ are given by

$$\begin{aligned} \widehat{\Sigma}_{S,N}^{(k,l)} &= \frac{1}{N} \sum_{i=1}^N z_k(\mathbf{x}_i) z_l(\mathbf{x}_i) \cdot \boldsymbol{\psi}(\mathbf{x}_i) \boldsymbol{\psi}(\mathbf{x}_i)^\top, \\ \widehat{\Sigma}_{S,T,N}^{(k,l)} &= \frac{1}{N} \sum_{i=1}^N z_k(\mathbf{x}_i) z_l(\mathbf{x}_i) \cdot \boldsymbol{\psi}(\mathbf{x}_i) \mathbf{w}(\mathbf{x}_i)^\top. \end{aligned}$$

We denote

$$s_{kl} = \frac{1}{N} \sum_{i=1}^N z_k(\mathbf{x}_i) z_l(\mathbf{x}_i) \quad \text{for all } k, l \in [d_z],$$

and observe that for $k \neq l$, $\mathbb{E}[s_{kl}] = 0$, and for $k = l$, $\mathbb{E}[s_{kk}] = 1$. We therefore observe and denote that

$$\mathbf{D}_S := \mathbb{E}_{\mathcal{D}(\eta_u)} \left[\widehat{\Sigma}_{S,N} \right] = \mathbf{I}_{d_z} \otimes \mathbf{C}_S(\eta_u), \quad \mathbf{D}_{S,T} := \mathbb{E}_{\mathcal{D}(\eta_u)} \left[\widehat{\Sigma}_{S,T,N} \right] = \mathbf{I}_{d_z} \otimes \mathbf{A}(\eta_u). \quad (26)$$

We further define the reminder fluctuation matrices around \mathbf{D}_S and $\mathbf{D}_{S,T}$:

$$\mathbf{E}_S = \widehat{\Sigma}_{S,N} - \mathbf{D}_S, \quad \mathbf{E}_{S,T} = \widehat{\Sigma}_{S,T,N} - \mathbf{D}_{S,T}, \quad (27)$$

where

$$\begin{aligned} \mathbf{E}_S = \left[\mathbf{E}_S^{(k,l)} \right]_{k,l=1}^{d_z} &= \begin{bmatrix} \widehat{\Sigma}_{S,N}^{(1,1)} - \mathbf{C}_S(\eta_u) & \widehat{\Sigma}_{S,N}^{(1,2)} & \cdots & \widehat{\Sigma}_{S,N}^{(1,d_z)} \\ \widehat{\Sigma}_{S,N}^{(2,1)} & \widehat{\Sigma}_{S,N}^{(2,2)} - \mathbf{C}_S(\eta_u) & \cdots & \widehat{\Sigma}_{S,N}^{(2,d_z)} \\ \vdots & \vdots & \ddots & \vdots \\ \widehat{\Sigma}_{S,N}^{(d_z,1)} & \widehat{\Sigma}_{S,N}^{(d_z,2)} & \cdots & \widehat{\Sigma}_{S,N}^{(d_z,d_z)} - \mathbf{C}_S(\eta_u) \end{bmatrix}, \\ \mathbf{E}_{S,T} = \left[\mathbf{E}_{S,T}^{(k,l)} \right]_{k,l=1}^{d_z} &= \begin{bmatrix} \widehat{\Sigma}_{S,T,N}^{(1,1)} - \mathbf{A}(\eta_u) & \widehat{\Sigma}_{S,T,N}^{(1,2)} & \cdots & \widehat{\Sigma}_{S,T,N}^{(1,d_z)} \\ \widehat{\Sigma}_{S,T,N}^{(2,1)} & \widehat{\Sigma}_{S,T,N}^{(2,2)} - \mathbf{A}(\eta_u) & \cdots & \widehat{\Sigma}_{S,T,N}^{(2,d_z)} \\ \vdots & \vdots & \ddots & \vdots \\ \widehat{\Sigma}_{S,T,N}^{(d_z,1)} & \widehat{\Sigma}_{S,T,N}^{(d_z,2)} & \cdots & \widehat{\Sigma}_{S,T,N}^{(d_z,d_z)} - \mathbf{A}(\eta_u) \end{bmatrix}. \end{aligned} \quad (28)$$

Again, following the proof of Lemma 2, the resolvent identity implies that

$$\begin{aligned} \widehat{\Sigma}_{S,N}^{-1} &= (\mathbf{D}_S + \mathbf{E}_S)^{-1} = \mathbf{D}_S^{-1} - \mathbf{D}_S^{-1} \mathbf{E}_S (\mathbf{D}_S + \mathbf{E}_S)^{-1} \\ &= \mathbf{D}_S^{-1} - \mathbf{D}_S^{-1} \mathbf{E}_S \mathbf{D}_S^{-1} + \mathbf{D}_S^{-1} \mathbf{E}_S \mathbf{D}_S^{-1} \mathbf{E}_S (\mathbf{D}_S + \mathbf{E}_S)^{-1}. \end{aligned} \quad (29)$$

Then, since $\mathbb{E}[\mathbf{E}_S] = \mathbf{0}_{d_S \times d_S}$ and $\mathbb{E}[\mathbf{E}_{S,T}] = \mathbf{0}_{d_S \times d_T}$, we have

$$\begin{aligned}
& \mathbb{E}_{\mathcal{S}_x} \left[\widehat{\Sigma}_{S,T,N}^\top \widehat{\Sigma}_{S,N}^{-1} \Sigma_{\phi_S, \eta_t} \widehat{\Sigma}_{S,N}^{-1} \widehat{\Sigma}_{S,T,N} \right] \\
&= \mathbb{E} \left[(\mathbf{D}_{S,T} + \mathbf{E}_{S,T})^\top (\mathbf{D}_S + \mathbf{E}_S)^{-1} (\mathbf{I}_{d_z} \otimes \mathbf{C}_S(\eta_t)) (\mathbf{D}_S + \mathbf{E}_S)^{-1} (\mathbf{D}_{S,T} + \mathbf{E}_{S,T}) \right] \\
&= \mathbf{D}_{S,T}^\top \mathbf{D}_S^{-1} (\mathbf{I}_{d_z} \otimes \mathbf{C}_S(\eta_t)) \mathbf{D}_S^{-1} \mathbf{D}_{S,T} + \mathbf{R}_N \\
&\quad + \mathbb{E} \left[\mathbf{E}_{S,T}^\top \mathbf{D}_S^{-1} (\mathbf{I}_{d_z} \otimes \mathbf{C}_S(\eta_t)) \mathbf{D}_S^{-1} \mathbf{E}_{S,T} \right] \quad (=: \mathbf{R}_{S,T}) \\
&\quad + \mathbb{E} \left[\mathbf{D}_{S,T}^\top \mathbf{D}_S^{-1} \mathbf{E}_S \mathbf{D}_S^{-1} (\mathbf{I}_{d_z} \otimes \mathbf{C}_S(\eta_t)) \mathbf{D}_S^{-1} \mathbf{E}_S \mathbf{D}_S^{-1} \mathbf{D}_{S,T} \right] \quad (=: \mathbf{R}_{S,S}) \\
&\quad - \mathbb{E} \left[\mathbf{D}_{S,T}^\top \mathbf{D}_S^{-1} \mathbf{E}_S \mathbf{D}_S^{-1} (\mathbf{I}_{d_z} \otimes \mathbf{C}_S(\eta_t)) \mathbf{D}_S^{-1} \mathbf{E}_{S,T} \right] \quad (=: \mathbf{R}_{S,S,T}) \\
&\quad - \mathbb{E} \left[\mathbf{E}_{S,T}^\top \mathbf{D}_S^{-1} (\mathbf{I}_{d_z} \otimes \mathbf{C}_S(\eta_t)) \mathbf{D}_S^{-1} \mathbf{E}_S \mathbf{D}_S^{-1} \mathbf{D}_{S,T} \right], \quad (=: \mathbf{R}_{S,T,S})
\end{aligned} \tag{30}$$

where $\|\mathbf{R}_N\|_2 = o_{\mathbb{P}}(1)$ for sufficiently large N ; \mathbf{E}_S and $\mathbf{E}_{S,T}$ are averages over N *i.i.d.* random matrices with $d_z \times d_z$ independent blocks. Therefore, when taking expectation for the second moments of \mathbf{E}_S and $\mathbf{E}_{S,T}$, the off-diagonal blocks in $\mathbf{R}_{S,T}, \mathbf{R}_{S,S}, \mathbf{R}_{S,S,T}, \mathbf{R}_{S,T,S} \in \mathbb{R}^{d_T \times d_T}$ vanish due to independence, and only the diagonal blocks remain, which are *i.i.d.* across $k \in [d_z]$. Notice that (26) implies that

$$\mathbf{D}_{S,T}^\top \mathbf{D}_S^{-1} (\mathbf{I}_{d_z} \otimes \mathbf{C}_S(\eta_t)) \mathbf{D}_S^{-1} \mathbf{D}_{S,T} = \mathbf{I}_{d_z} \otimes \mathbf{C}_{T,S}(\eta_t, \eta_u).$$

Also, we recall that the fourth moment of any Gaussian random vector $\mathbf{g} \sim \mathcal{N}(\mathbf{0}, \mathbf{I}_d)$ satisfies for any fixed matrix $\mathbf{M} \in \mathbb{R}^{d \times d}$,

$$\mathbb{E} \left[(\mathbf{g} \mathbf{g}^\top)^2 \right] = (d+2) \mathbf{I}_d, \quad \mathbb{E} \left[(\mathbf{g} \mathbf{g}^\top) \mathbf{M} (\mathbf{g} \mathbf{g}^\top) \right] = \text{tr}(\mathbf{M}) \mathbf{I}_d + \mathbf{M} + \mathbf{M}^\top. \tag{31}$$

Define a function $g : \mathbb{R}^{d_T \times d_T} \rightarrow \mathbb{R}$ as

$$g(\mathbf{A}) = \frac{1}{n} \text{tr} \left(\mathbf{A} \mathbb{E}_{\tilde{\mathcal{S}}} \left[\tilde{\Sigma}_{T,n}^{-1} \right] \right).$$

Then, we have

$$\begin{aligned}
& \frac{1}{n} \text{tr} \left(\mathbb{E}_{\mathcal{S}_x} \left[\widehat{\Sigma}_{S,T,N}^\top \widehat{\Sigma}_{S,N}^{-1} \Sigma_{\phi_S, \eta_t} \widehat{\Sigma}_{S,N}^{-1} \widehat{\Sigma}_{S,T,N} \right] \mathbb{E}_{\tilde{\mathcal{S}}} \left[\tilde{\Sigma}_{T,n}^{-1} \right] \right) \\
&= g(\mathbf{I}_{d_z} \otimes \mathbf{C}_{T,S}(\eta_t, \eta_u)) + g(\mathbf{R}_{S,T}) + g(\mathbf{R}_{S,S}) - g(\mathbf{R}_{S,S,T}) - g(\mathbf{R}_{S,T,S}) + o_{\mathbb{P}}(1),
\end{aligned}$$

where given the $\mathbf{I}_{d_z} \otimes \mathbf{C}_{T,S}(\eta_t, \eta_u)$ structure, Lemma 2 then implies that under the proportional asymptotic limit,

$$g(\mathbf{I}_{d_z} \otimes \mathbf{C}_{T,S}(\eta_t, \eta_u)) \xrightarrow{\mathbb{P}} \gamma_z \text{tr} \left(\mathbf{C}_{T,S}(\eta_t, \eta_u) \mathbf{C}_T(\eta_\ell)^{-1} \right).$$

Let $\mathbf{M} := \mathbf{C}_S(\eta_t) \mathbf{C}_S(\eta_u)^{-1} \in \mathbb{R}^{p_S \times p_S}$ and $\mathbf{M}' := [\mathbf{M}]_{2:p_S, 2:p_S}$. Recall from (30) that $\mathbf{R}_{S,T} = \mathbb{E} \left[\mathbf{E}_{S,T}^\top \mathbf{D}_S^{-1} (\mathbf{I}_{d_z} \otimes \mathbf{C}_S(\eta_t)) \mathbf{D}_S^{-1} \mathbf{E}_{S,T} \right]$, (31) and (14), along with the proof of Lemma 2 imply that

$$g(\mathbf{R}_{S,T}) \xrightarrow{\mathbb{P}} \gamma_z \nu_z \left(p_T \text{tr}(\mathbf{M}) + \frac{2}{\sigma_\xi^2} \text{tr}(\mathbf{M}' \boldsymbol{\Xi}^\top \boldsymbol{\Xi}) + C_S \frac{(\eta_u - \eta_\ell)^2 \|\boldsymbol{\mu}_T\|_2^2}{\sigma_\xi^2} \right),$$

for some constant $C_S > 0$ independent of d_z, N . Analogously, we have

$$\begin{aligned} g(\mathbf{R}_{S,S}) &\xrightarrow{\mathbb{P}} \gamma_z \nu_z \left(p_{T \wedge S} \text{tr}(\mathbf{M}) + \frac{2}{\sigma_\xi^2} \text{tr}(\mathbf{M}' \boldsymbol{\Xi}^\top \boldsymbol{\Xi}) + C_S \frac{(\eta_u - \eta_\ell)^2 \|\boldsymbol{\mu}_T\|_2^2}{\sigma_\xi^2} \right), \\ g((\mathbf{R}_{S,S,T})) &\xrightarrow{\mathbb{P}} \gamma_z \nu_z \left(p_{T \wedge S} \text{tr}(\mathbf{M}) + \frac{2}{\sigma_\xi^2} \text{tr}(\mathbf{M}' \boldsymbol{\Xi}^\top \boldsymbol{\Xi}) + C_S \frac{(\eta_u - \eta_\ell)^2 \|\boldsymbol{\mu}_T\|_2^2}{\sigma_\xi^2} \right) \\ g((\mathbf{R}_{S,T,S})) &= g((\mathbf{R}_{S,S,T})). \end{aligned}$$

Overall, at the proportional asymptotic limit,

$$\begin{aligned} &\frac{1}{n} \text{tr} \left(\mathbb{E}_{\mathcal{S}_x} \left[\widehat{\boldsymbol{\Sigma}}_{S,T,N}^\top \widehat{\boldsymbol{\Sigma}}_{S,N}^{-1} \boldsymbol{\Sigma}_{\phi_S, \eta_t} \widehat{\boldsymbol{\Sigma}}_{S,N}^{-1} \widehat{\boldsymbol{\Sigma}}_{S,T,N} \right] \mathbb{E}_{\tilde{\mathcal{S}}} \left[\widetilde{\boldsymbol{\Sigma}}_{T,n}^{-1} \right] \right) \\ &\xrightarrow{\mathbb{P}} \gamma_z \text{tr}(\mathbf{C}_{T,S}(\eta_t, \eta_u) \mathbf{C}_T(\eta_\ell)^{-1}) + \gamma_z \nu_z (p_T - p_{T \wedge S}) \text{tr}(\mathbf{C}_S(\eta_t) \mathbf{C}_S(\eta_u)^{-1}). \end{aligned}$$

□

D Additional Experimental Details

D.1 Dataset Statistics

In this work, we construct three distinct splits for each of the four datasets, Waterbirds [Sagawa et al., 2020], BFFHQ [Lee et al., 2021], ImageNet-9 [Xiao et al., 2020], and BG-COCO. Specifically, each dataset is partitioned into a group-imbalanced training set \mathcal{D}_1 , a group-balanced training set \mathcal{D}_2 , and a group-balanced test set \mathcal{D}_3 . The minority group proportion in \mathcal{D}_1 , \mathcal{D}_2 , and \mathcal{D}_3 is η_o , 0.5, and 0.5, respectively. Across different real-world experiments in the paper, we vary the group proportions (η_ℓ and η_u) as well as the sample sizes (n and N). We first summarize the dataset statistics for each benchmark, and then describe how \mathcal{D}_1 to \mathcal{D}_3 are utilized in different experimental setups.

Waterbirds statistics. The Waterbirds [Sagawa et al., 2020] dataset is designed to capture spurious correlations between natural backgrounds and bird labels, with $\eta_o = 0.05$. Table 3 reports the detailed group distributions across \mathcal{D}_1 to \mathcal{D}_3 . Following Sagawa et al. [2020], we supplement additional samples for the minority groups (waterbird, land) and (landbird, water) in the same manner as the original dataset, due to the limited size of the raw data.

Split	(waterbird, water)	(waterbird, land)	(landbird, water)	(landbird, land)	Total
\mathcal{D}_1	1,057	56	184	3,498	4,795
\mathcal{D}_2	1,804	1,804	1,804	1,804	7,216
\mathcal{D}_3	451	451	451	451	1,804

Table 3: Dataset statistics for Waterbirds. Each column corresponds to a group, and the last column gives the total sample count.

BFFHQ statistics. The BFFHQ [Lee et al., 2021] dataset is designed to capture spurious correlations between age and gender labels, with $\eta_o = 0.005$. Table 4 reports the detailed group distributions across \mathcal{D}_1 to \mathcal{D}_3 . Due to the limited size of the minority groups in the raw data, our splits are constructed from de-duplicated samples across multiple BFFHQ subsets.

Split	(young, female)	(young, male)	(old, female)	(old, male)	Total
\mathcal{D}_1	9,552	48	48	9,552	19,200
\mathcal{D}_2	790	790	790	790	3,160
\mathcal{D}_3	198	198	198	198	792

Table 4: Dataset statistics for BFFHQ. Each column corresponds to a group, and the last column gives the total sample count.

ImageNet-9 statistics. The ImageNet-9 [Xiao et al., 2020] dataset is designed to capture spurious correlations between object and background labels. Different from Waterbirds and BFFHQ, ImageNet-9 is a 9-class classification task over categories dog, bird, wheeled vehicle, reptile, carnivore, insect, musical instrument, primate, and fish. The original dataset provides two variants, mixed-same and mixed-rand. In the mixed-same version, each image background is replaced with a background from an image of the same class, thus preserving spurious correlations; in the mixed-rand version, the background is randomized and contains no information about the true label. These two variants correspond to minority group proportions of 0 and 0.5, respectively. Table 5 reports the dataset statistics across \mathcal{D}_1 to \mathcal{D}_3 . Based on this table, we set $\eta_o = 0$. Note that ImageNet-9 does not have a well-defined group structure under either the mixed-same or mixed-rand settings. Therefore, we do not report worst-group accuracy for this dataset.

Split	mixed-same	mixed-rand	Total	Per-class
\mathcal{D}_1	4,050	0	4,050	450
\mathcal{D}_2	0	3,240	3,240	360
\mathcal{D}_3	0	810	810	90

Table 5: Dataset statistics for ImageNet-9. Within each split, the nine classes have identical counts.

BG-COCO statistics. The BG-COCO dataset is a self-generated benchmark designed to capture spurious correlations between cats/dogs from COCO [Lin et al., 2014] and indoor/outdoor scenes from Places [Zhou et al., 2017]. Specifically, we define the indoor/outdoor split as living room, dining room (indoor) and park (outdoor). By construction, cats are aligned with indoor scenes and dogs with outdoor scenes. Table 6 reports the detailed group distributions across \mathcal{D}_1 to \mathcal{D}_3 . Based on this table, we set $\eta_o = 0.05$.

Split	(cat, indoor)	(cat, outdoor)	(dog, indoor)	(dog, outdoor)	Total
\mathcal{D}_1	1,900	100	100	1,900	4,000
\mathcal{D}_2	1,000	1,000	1,000	1,000	4,000
\mathcal{D}_3	250	250	250	250	1,000

Table 6: Dataset statistics for BG-COCO. Each column corresponds to a group, and the last column gives the total sample count.

Across all four datasets, we construct training and evaluation splits as follows. When either η_ℓ or η_u is fixed η_o , samples are drawn from \mathcal{D}_1 with the desired size N (for unlabeled data) or n (for labeled data). When either η_ℓ or η_u is fixed to 0.5, balanced samples are instead drawn from \mathcal{D}_2 . Several experiments involve fixing η_ℓ while varying η_u . In this setting, if necessary,

we keep the labeled data unchanged and supplement the unlabeled data with additional samples independently drawn from \mathcal{D}_1 or \mathcal{D}_2 , while ensuring that the total unlabeled sample size N remains constant across different η_u . The balanced dataset \mathcal{D}_3 is reserved for testing, and when required, we further split 20% of \mathcal{D}_3 as a separate validation set.

D.2 Results for Interpreting W2S under Spurious Correlations

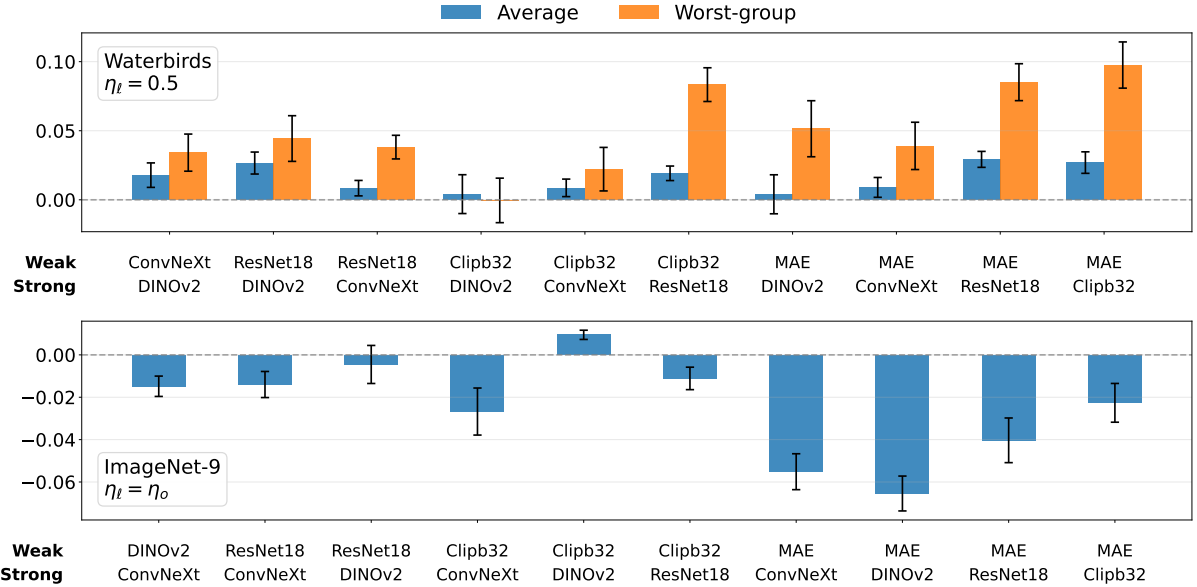


Figure 5: Top: On the Waterbirds dataset, the change in W2S gain (value at $\eta_u = 0.5$ minus value at $\eta_u = 0$) across all teacher–student pairs with fixed $\eta_\ell = 0.5$. Bottom: On the ImageNet-9 dataset, the change in W2S gain (value at $\eta_u = 0.5$ minus value at $\eta_u = \eta_o$) across all teacher–student pairs with fixed $\eta_\ell = \eta_o$. ImageNet-9 does not have a clearly defined worst group and is therefore omitted from the bottom panel.

Dataset	# of model pairs with increased W2S gain	
	Average accuracy	Worst group accuracy
Waterbirds	10/10	10/10
BFFHQ	10/10	9/10
BG-COCO	9/10	10/10
ImageNet-9	7/10	—

Table 7: Proportion of teacher-student pairs that exhibit an increase in W2S gain as η_u increases from 0 to the maximum feasible value of η_u (Waterbirds: 0.5, BFFHQ: 0.23, BG-COCO: 0.5, ImageNet-9: 0.4) when $\eta_\ell = 0.5$, summarized across all datasets. ImageNet-9 has no well-defined worst group, so only average accuracy is reported.

In Section 3.2, we primarily presented how the average W2S gain across all teacher–student pairs varies with increasing η_u on each dataset. Here, we further provide results for individual model pairs. Specifically, Figure 5 compares the difference in W2S gain between the group-balanced ($\eta_\ell = 0.5$) and group-imbalanced ($\eta_\ell = \eta_o$) settings on selected datasets. Table 7 summarizes, for $\eta_\ell = 0.5$, the proportion of model pairs that exhibit an increase in W2S gain as η_u increases

Dataset	# of model pairs with decreased W2S gain	
	Average accuracy	Worst group accuracy
Waterbirds	7/10	8/10
BFFHQ	8/10	7/10
BG-COCO	8/10	7/10
ImageNet-9	9/10	—

Table 8: Proportion of teacher-student pairs that exhibit a decrease in W2S gain as η_u increases from η_o to 0.5 when $\eta_\ell = \eta_o$, summarized across all datasets. ImageNet-9 has no well-defined worst group, so only average accuracy is reported.

from 0 across all datasets. Table 8 summarizes, for $\eta_\ell = \eta_o$, the proportion of model pairs that exhibit a decrease in W2S gain as η_u increases from η_o across all datasets. These results further validate our theoretical analysis in Section 2.2, which predicts that in most cases the larger the gap between η_u and η_ℓ , the smaller the resulting W2S gain.

D.3 Results for Enhanced W2S

Model training. Enhanced-W2S improves upon vanilla W2S by retraining the strong student after the initial W2S fine-tuning. First, we select a fraction $p \in (0, 1]$ of $\hat{\mathcal{S}}$ consisting of those samples for which the student exhibits the lowest prediction entropy. Second, we apply the GCE loss $\mathcal{L}_{\text{GCE}}(\mathbf{x}_i, \hat{y}_i; q)$ with parameter $q \in (0, 1]$ to each selected sample $(\mathbf{x}_i, \hat{y}_i)$. We tune the hyperparameters by grid search over $p \in \{0.2, 0.4, 0.6, 0.8, 1.0\}$ and $q \in \{0, 0.2, 0.7\}$, where $q = 0$ corresponds to the CE loss (i.e., the $q \rightarrow 0$ limit of GCE). To avoid a trivial overlap with the vanilla W2S baseline, $(p, q) = (1, 0)$ is excluded from the Enhanced-W2S search space. In the case of $(\eta_\ell, \eta_u) = (\eta_o, 0.5)$, we further restrict the subset ratio to $p \in \{0.2, 0.4, 0.6\}$ to emphasize the role of high-confidence subsets in filtering for the majority group. Each run of Enhanced-W2S is repeated with multiple random seeds, and the reported results are obtained by averaging across seeds.

Dataset	η_ℓ	η_u	Mean relative improvement (%)	
			Average Accuracy	Worst Group Accuracy
Waterbirds	0.5	η_o	6.32	10.12
	η_o	0.5	7.72	32.15
BFFHQ	0.5	η_o	5.52	4.06
	η_o	0.5	3.12	3.57
BG-COCO	0.5	η_o	10.51	11.76
	η_o	0.5	4.50	3.71
ImageNet-9	0.5	η_o	12.23	—
	η_o	0.5	11.23	—

Table 9: Mean relative improvement (%) of Enhanced-W2S over vanilla W2S, averaged across selected teacher-student pairs, for both average accuracy and worst group accuracy. For each dataset, we select all model pairs whose relative strength relationship remains consistent across different (η_ℓ, η_u) settings.

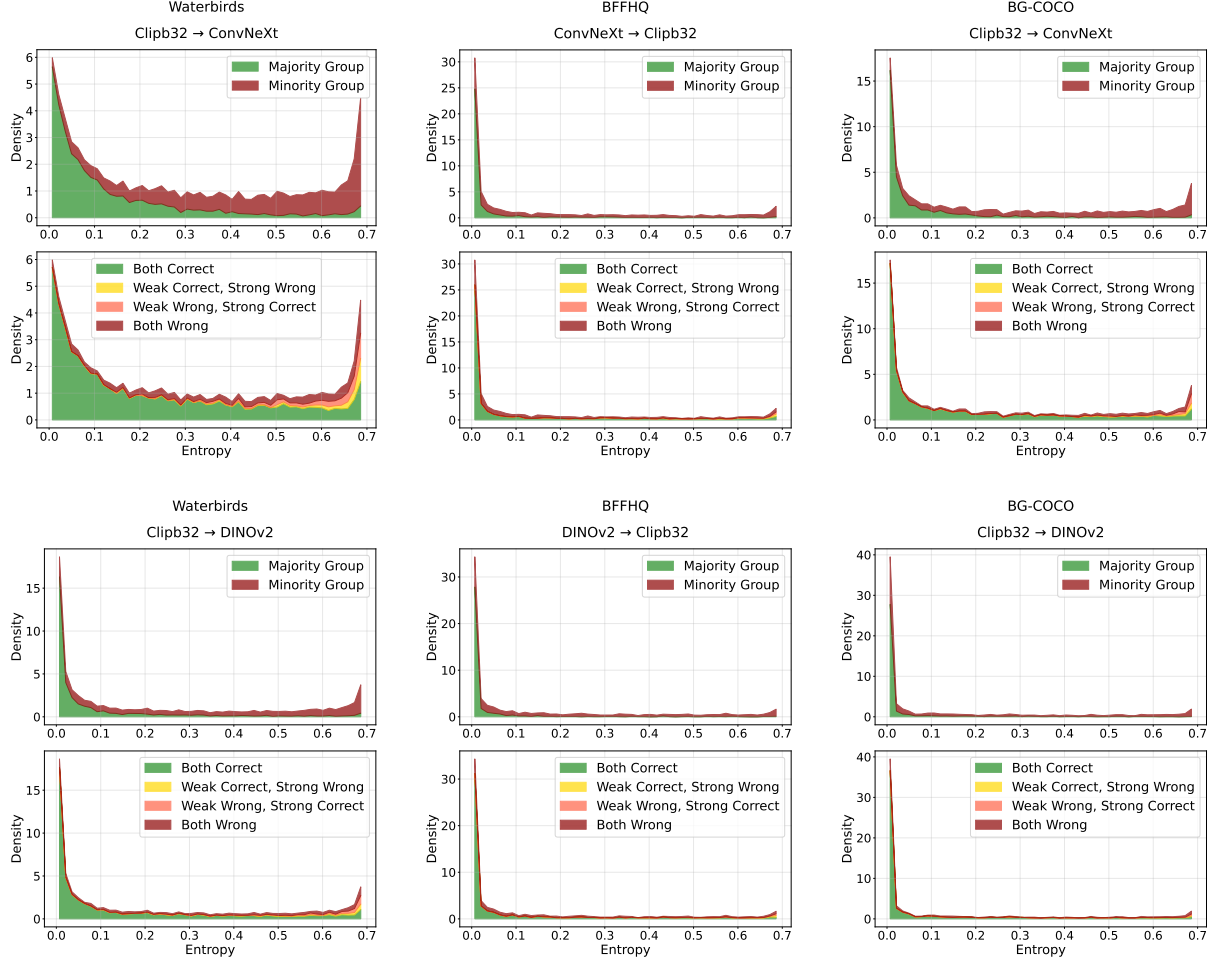


Figure 6: Student confidence on unlabeled data as stacked density plots of predictive entropy ($\eta_\ell = \eta_o$, $\eta_u = 0.5$). Each panel shows the student’s predictive entropy (after W2S fine-tuning), visualized as two stacked density plots: (top) split by group (majority vs. minority) and (bottom) split by prediction correctness of the weak teacher and the strong student. Columns correspond to datasets (Waterbirds, BFFHQ, BG-COCO). Rows correspond to model pairs: (ConvNeXt, Clipb32) and (Clipb32, DINOv2).

Role of confidence-based selection. When $(\eta_\ell, \eta_u) = (\eta_o, 0.5)$, Figure 6 shows that samples with high student confidence (i.e., low predictive entropy) after W2S fine-tuning are almost exclusively drawn from the majority group, and furthermore are nearly always assigned the correct pseudolabels by both the weak teacher and the strong student. At the same time, Theorem 2 predicts that reducing η_u from 0.5 directly increases the W2S gain. These two observations together suggest that confidence-based selection provides significant benefits for improving W2S performance in the setting $(\eta_\ell, \eta_u) = (\eta_o, 0.5)$.

Mean relative gains. Table 9 summarizes the mean relative improvement of Enhanced-W2S over vanilla W2S, averaged across all teacher–student pairs. Consistent with the main text, our method achieves clear gains under both average accuracy and worst group accuracy.